Analysis of Potential for Titanium Liner Buckling after Proof in a Large Kevlar/Epoxy COPV

S. Leigh Phoenix [1]
Cornell University, Ithaca, NY, 14853, USA

and

Michael T. Kezirian [2]
The Boeing Company, Houston, TX, 77058

ABSTRACT. We analyze the potential for liner buckling in a 40-in Kevlar49/epoxy overwrapped spherical pressure vessel (COPV) due to long, local depressions or 'valleys' in the titanium liner, which appeared after proof testing (autofrettage). We begin by presenting the geometric characteristics of approximately 20 mil (0.02 in.) deep depressions measured by laser profilometry in several vessels. While such depths were more typical, depths of more than 40 mils (0.02 in.) were seen near the equator in one particular vessel. Such depressions are largely the result of overlap of the edges of overwrap bands (with rectangular cross-section prepreg tows) from the first or second wrap patterns particularly where they start and end. We then discuss the physical mechanisms of formation of the depressions during the autofrettage process in terms of uneven void compaction in the overwrap around the tow overlap lines and the resulting 10-fold increase in through-thickness stiffness of the overwrap. We consider the effects of liner plastic yielding mechanisms in the liner on residual bending moments and interface pressures with the overwrap both at the peak proof pressure (~6500 psi) and when reducing the pressure to 0 psi. During depressurization the Bauschinger phenomenon becomes very important whereby extensive yielding in tension reduces the magnitude of the yield threshold in compression by 30 to 40%, compared to the virgin annealed state of the liner titanium. In the absence of a depression, the liner is elastically stable in compression even at liner-overwrap interface pressures nominally 6 times the ~ 1000 psi interface pressure that exists at 0 psi. Using a model based on a plate-on-an-elastic-foundation, we develop an extensive analysis of the possible destabilizing effects of a frozen-in valley. The analysis treats the modifying effects of the residual bending moments and interface pressures remaining after the proof hold as well as the Bauschinger effect on the compressive yield threshold. The key result is that depression depths of up to 40 mils can be tolerated, but above 40 mils, the Bauschinger effect drives destabilization, and buckling becomes increasingly likely depending on the details of depression formation during autofrettage. It is almost certain that destabilization and buckling will occur for depression depths beyond 55 mils. The main equations and formulas for treating the various phases of depression development and potential buckling, are only briefly outlined in the paper, but are available from the authors.

I. Introduction

Proof testing of composite-overwrapped pressure vessels (COPVs) that have a metal liner typically result in plastic yielding of the liner material so that upon returning to zero pressure, the liner is in a state of hoop compression under an overwrap-liner interface pressure. The main benefit of this autofrettage effect is that during COPV service under steady pressure, which may involve cycling from zero pressure to maximum operating pressure, the liner stays within the elastic state and fatigue life is greatly extended. At the same time, placing the liner in a compressive state when unpressurized introduces the risk of local buckling. Even if unbuckled after the

---

[1] Prof., Department of Theoretical and Applied Mechanics, Cornell University, Ithaca NY 14853.
[2] Safety Engineer, and Adjunct Associate Professor, University of Southern California, and AIAA Associate Fellow.

proof test, the potential for liner buckling may remain in marginal vessels should an unpressurized vessel with a carbon or Kevlar/epoxy fiber overwrap be raised in temperature, since the overwrap and liner have opposite coefficients of thermal expansion. Although designing against liner buckling is ostensibly straightforward, several factors may increase the risk such as variability in liner and overwrap mechanical properties, bonding between the liner and overwrap (if required for stability), and irregularities in tow and band packing.

In this paper we develop an analysis of the potential for liner buckling in a 40-in diameter, Kevlar49/epoxy COPV with a 0.74 inch thick overwrap and 0.105 inch thick titanium liner. Some vessels were found to have local depressions or valleys (dents) in the titanium liner that appeared after proof testing. We begin by presenting the geometric characteristics of approximately 20 mils (0.02 in.) deep depressions measured on the inside liner surface by laser profilometry (and seen as bumps). While such depths are more typical, depressions of more than 40 mils (0.02 in.) were seen near the equator in one particular vessel. These depressions are believed to be the result of overlap of the edges of the overwrap bands from the first wrap patterns particularly where they begin and terminate. The physical mechanisms of formation of the depressions during the autofrettage process involve uneven void compaction and overwrap stacking at the locations where bands overlap, especially at the beginning and ends of wrap patterns. We also discuss the consequences of extensive liner plastic yielding mechanisms on residual bending moments and interface pressures both at the peak proof pressure of ~ 6500 psi, and during depressurization to 0 psi after autofrettage. In the latter case the Bauschinger phenomenon on lowering the yield threshold becomes very important since the extensive yielding in tension reduces the magnitude of the yield threshold in compression by 30 to 40%, compared to the virgin annealed state.

To provide a context for the detailed analysis and modeling, we performed a preliminary analysis of the in-plane buckling loads and critical half-wavelength scales from various results from classical buckling theory, including (i) a free-standing sphere under external pressure, (ii) a short cylinder under a uniaxial compressive load, and (iii) a plate on an elastic foundation with hinged boundary conditions. By comparing the results of these various cases we found that the analysis of the potential for buckling of the liner in these liner/overwrap configurations reduces to considering the behavior of a rectangular hinged plate (a 0.105 in. thick liner section spanning zero bending moment lines) on an elastic foundation (provided by the 0.74 in. thick overwrap) and with a "frozen-in" depression or valley that also has residual bending moment and interface pressure fluctuations remaining after plastic yielding during autofrettage. In the absence of a depression, we find that the liner is elastically stable in compression at liner-overwrap interface pressures nominally six times the approximately 1000 psi that exists at zero vessel pressure after autofrettage. The analysis treats the modifying effects of the residual bending moments and interface pressures remaining after the proof hold at peak pressure, as well as the Bauschinger attenuation effect on the plastic yield threshold in compression. The main equations and formulas for treating the various phases of the depression development, and potential buckling during depressurization, are only briefly outlined in the paper, but are available from the authors in more detail.

First we discuss the fundamental differential equations and their solution for transverse liner elastic deformation due to application of a narrow perpendicular line load. This is done both for the case of in-plane tension, as occurs during autofrettage, and in-plane compression, as occurs during subsequent depressurization. Using independently determined material stiffness parameters, we calculate depression or valley profiles that match well those experimentally observed using laser profilometry. A crucial aspect is that the transverse (through-thickness) stiffness of the overwrap in this initial pressurization phase is governed by overwrap porosity from extensive voids, and thus, is an order of magnitude less that the transverse stiffness that exists after void collapse and during depressurization. This key aspect is the reason why permanent volume growth from autofrettage varies by more than a factor of two among these vessels.

Next, we determine mathematical results for interface pressure and residual bending moment profiles that remain after liner yielding is complete at the maximum proof pressure, which is held for a few minutes. An important aspect is the calculation of the extent of dispersion or spreading of the sharp spike in interface pressure, which results from liner yielding and flattening of the overwrap bump. Also important is the fact that force balance requires that the integral of the pressure fluctuation must sum to zero so that the pressure peak must be compensated by pressure reductions on each side of the pressure hump of the displacement valley. Through two integrations across the locally parabolic pressure peak, the dispersion smoothes out the pointed profile of the bending moment (a characteristic of line loads such as in three-point bending), replacing it with a locally parabolic shape. This dispersion has virtually no effect on the depression profile shape since this shape involves two further integrations of the bending moment in the underlying fourth order differential equation. However it smoothes out the pressure fluctuations and make it easier to appreciate the local interface pressure loss with increasing depression depth, which is a precursor to buckling. Within physically reasonable limits, the actual breadth of the dispersion has very little effect on the main predictions regarding the onset of buckling.

Third, we calculate the changes in the interface pressure and bending moment profile from the state at peak proof pressure, as well as changes in the depression shape and depth that occur during depressurization of the COPV from the peak proof pressure down to zero pressure. The key driving shape in the equations is the depression shape for the tensioned liner during the pressure buildup of autofrettage, which occurs at a low transverse stiffness of the overwrap. However, in the depressurization, transverse overwrap stiffness becomes the high stiffness of the compacted overwrap with voids removed. Finally we discuss the key framework for superimposing the results for various stages of the autofrettage cycle, particularly the depressurization phase. Also considered are criteria that allow final assessment of the likelihood of liner buckling for various values of initial 'frozen-in" depression depth.

The key result is that depression depths of up to 40 mils can be tolerated by the liner. Above 40 mils, the Bauschinger effect dominates and destabilization and buckling becomes increasingly likely depending on the details of depression formation during the proof pressurization. Whatever the mechanical property variations for a vessel, it is almost certain that destabilization and buckling will occur for depression depths beyond 55 mils.

II. Laser Profilometry Measurements and Potential Buckling Mechanisms

From laser profilometry on the inside surfaces of both 26 and 40 inch Kevlar/epoxy COPVs at zero pressure, such valleys (referenced from the overwrap side), have been seen in certain vessels. These depressions typically have a characteristic width of a few inches along the liner surface and in some cases tend to exhibit a modest overshoot on each side, i.e., small hills flanking the valley, suggestive of mild oscillatory behavior in the disturbance as it dies out. An illustration of such a depressions found in a 26 in. spherical vessel is shown in Figure 1, where the horizontal axis is circumference measured in degrees and the vertical axis is degrees latitude relative to the equator at 0 degrees [1]. The smaller ripples have width 1.26 inches, consistent with the width of the bands in the wrap patterns.
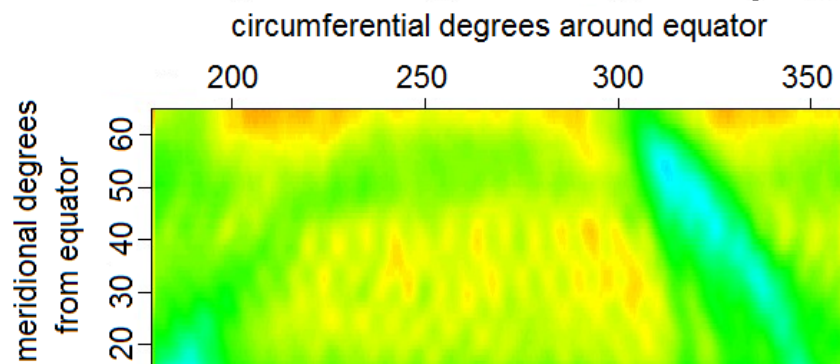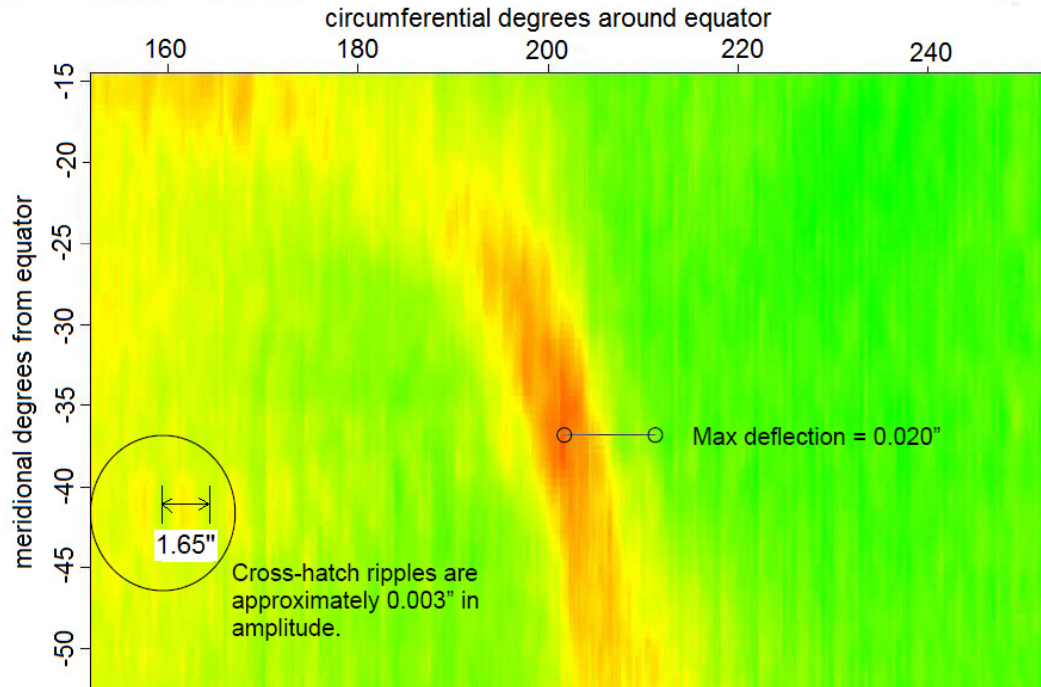

Figure 1: Profilometry map of surface depression (blue) observed in a 26 in. Kevlar/epoxy COPV with a titanium liner. The depression, measured at NASA-JSC WSTF [1] was 22 mils deep.

Figure 2 shows a similar depression observed in a 40 inch spherical Kevlar 49/epoxy COPV. A somewhat surprising feature is that the ripples have spacings much more consistent with the bands in the 2nd, and higher wrap patterns than in the 1st wrap pattern. The former are about 1.65 inches wide while the latter are 1.05 inches wide. An interesting issue is whether the small ripple wavelength is more consistent with and somewhat excited by a natural buckling wavelengths of the overwrap-liner combination. Nonetheless the span of the main depression appears to be significantly larger than of the periodic ripples.

Figure 3 shows the dimensional characteristics of a depression. The liner is put into compression when the vessel pressure is reduced to zero after autofrettage, and thus, a critical question arises regarding the possibility of buckling, and its dependence on the depth and width of the valley, as well as other characteristics of the liner and overwrap. Since the liner is not bonded to the overwrap (in fact the surface has a release agent by design), the possibility exists that the liner will buckle if the depression depth formed at proof, exceeds some critical value whereby the liner loses the elastic support of the overwrap and separates. Of primary interest are the conditions under which such liner buckling can occur, and "safe" conditions under which the liner will be stable.

Figure 2: **Profilometry map of a surface depression (red region) observed in a 40 in. diameter Kevlar/epoxy COPV with a titanium liner. The depression, measured at NASA-JSC WSTF [1], was 20 mils deep.**
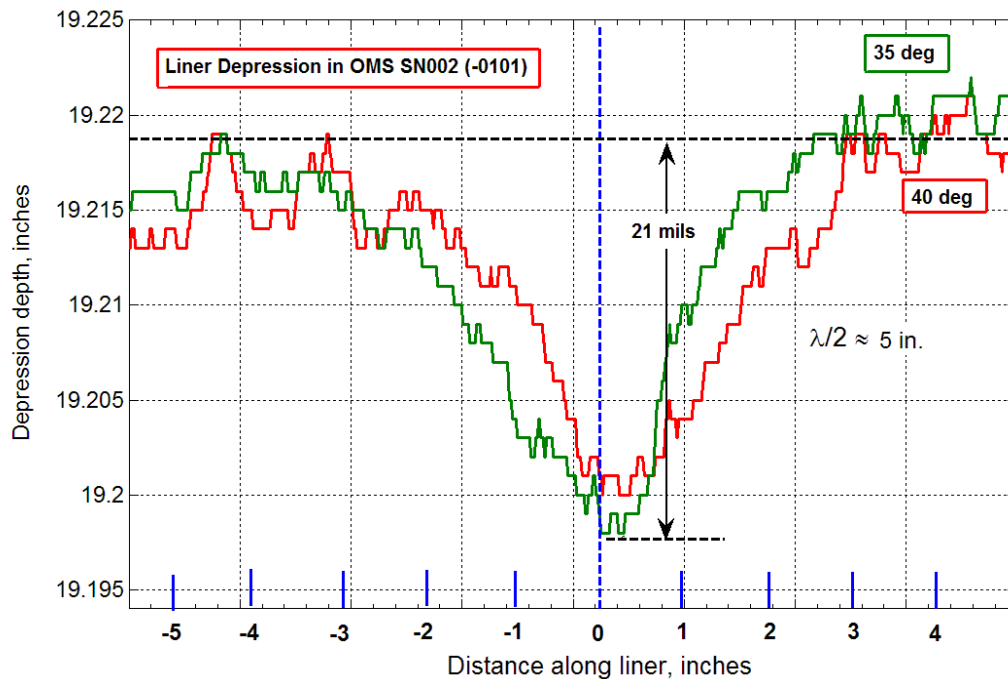

Figure 3. Characteristics of the cross-section of an approximately 20-mil depression in a vessel [1].

A. Mechanisms of Initial Formation of the Liner Depression

In modeling the effects of such a liner depression, the first issue to consider is the conditions under which a depression forms as well as the "frozen-in" geometric bending moment and interface pressure characteristics it inherits from autofrettage. Immediately after curing the freshly wound vessel and before autofrettage, there are no

obvious mechanical reasons why such depressions should occur. However during the pressure build-up of the autofrettage cycle, which includes a 2 to 5 minute hold at 3000 to 3500 psi and a 2 minute hold at the proof pressure of 6520 psi, the conditions are favorable to form such depressions. Interpreting experiments on through-thickness deformation of vessel cross-sections it is found that, the transverse compressive overwrap stiffness through the thickness before autofrettage is up to a factor of 10 lower than it is after autofrettage (e.g., about 25,000 psi versus 250,000 psi). The apparent cause of this large increase is permanent collapse of air voids in the overwrap as the interface pressure increases during autofrettage.

From plots of growth in boss-to-boss length versus pressure, there is strong evidence that much of the void collapse already occurs before or at the hold pressure of 3000 to 3500 psi during autofrettage, even before the tensile yield strain in the liner has been reached. An important observation is that the permanent volume growth resulting from the proof process is from 1.5 to 2.25 times larger that calculated from both FEA and membrane mechanics models of the vessel proof process, again the likely result of compression of entrained air voids. This discrepancy translates into liner radial displacements of about 40 mils beyond predictions, or about 6% of the 0.74 in. overwrap thickness. An uneven void distribution in the overwrap is likely where overlap of bands in the first wrap occurs as they travel from the equator to the boss zone, particularly in starting and terminating wrap patterns and circuits. This makes it possible for local bumps in the overwrap to occur as voids on each side are collapsed. Coincidentally depressions of 20 mils, as shown above in Figures 1 to 3, are approximately the thickness of two stacked, Kevlar/epoxy prepreg tows made from 4560 denier yarn. Stacking of multiple overlaps is possible where wrap patterns begin and end if special effort is not made to ensure offset positioning. Thus depressions deeper than 20 mils are possible, and a depression of 40 mils was observed in one vessel near the equator.

An important aspect is the permanent cross-sectional shape of such "frozen-in" depressions or valleys in the liner, including depth, width and length. Extensive liner yielding in tension occurs during proof and the final plastic strain at the end of the 2 minute proof hold at 6520 psi is larger than the elastic strain at yield onset, by 15 to 40% (i.e., total strain is 2.15 to 2.4 times the yield strain). This relieves most of elastic bending moment induced by the change in liner curvature as the depression forms. The residual bending moment and associated residual interface pressure disturbance is critical to assessing the likelihood of buckling as the vessel pressure is lowered to zero and the liner is put in compression. This compression results in approximately a 1000 psi average interface pressure (in both 40 inch and 26 inch diameter COPV)) between the overwrap and liner, which is crucial to the liner's stability as the overwrap acts as an elastic foundation. If this interface pressure locally falls to zero for larger depression depths, elastic foundation support is lost and the conditions become favorable for liner buckling.

B. Potential Mechanisms of Buckling and Inherent Resistance Factors

Without the elastic foundation support of the overwrap, the liner is not capable of supporting the approximately 1000 psi interface pressure that exists after autofrettage when the vessel returns zero pressure. As we show later, the critical buckling pressure of the stand-alone liner is at most 600 psi with a critical half wavelength of about 2.5 inches. Thus to prevent buckling, the liner relies on the lateral support of the overwrap as an elastic foundation. Maintaining a positive interface pressure is crucial to this support mechanism, since the liner and overwrap will then act as though they are bonded. An appreciation of the effectiveness of the overwrap in preventing liner buckling can be obtained from analysis of a plate on an elastic foundation, as we develop shortly. We find that the reinforcing effect is by a factor of about 6 meaning that the liner could nominally sustain interface pressures of close to 5,000 psi (assuming it did not yield in hoop compression) as part of the coupled liner-overwrap system, and the half wavelengths of buckling would be about 1 inch. The fact that the liner is *not* bonded to the interface means that the likelihood of liner buckling is closely tied to the likelihood of loss of interface pressure and subsequent liner separation from the unbonded overwrap. By itself, this local loss of interface pressure may not be sufficient for buckling. It is also necessary that characteristic length over which contact has been lost, and the distance between zero bending moment points, must also match the characteristic buckling length of an unsupported plate-like region of the liner with hinged boundary conditions. From buckling theory for free-standing plates, it can be shown that for in-plane compressive loads that exist at zero vessel pressure (about 10,000 lb./in), the characteristic, half-wavelength for buckling is about 2 inches. Thus a model for buckling of the liner must consider the likelihood such conditions will be realized when the depression depths and widths are of sufficient magnitude.

As mentioned, a crucial aspect of when such conditions might arise is the magnitudes of local residual bending moments and interface pressure increases that result from the formation of such a depression during autofrettage. As the depression forms there is extensive liner yielding that occurs that will relax the natural bending moments from liner curvature changes, whether elastic or plastic. It can be shown that for a laboratory section of the liner in three-point bending the maximum elastic bending moment possible (before yielding on the surface begins at about

128 ksi) is about 240 lb-in./in. and the ultimate plastic bending moment is 3/2 times this value, or 360 lb-in. per inch. However these large magnitudes are only possible if the in-plane liner loads average to zero, which is not the case during autofrettage where the in-plane strain of the liner becomes more than double the elastic yield strain when the depression formation process is active. Thus more than half of the elastic bending moment from the axisymmetric, triangle-shaped bending stress distribution is flattened and eliminated (all on one side and part of the other side), and for deeper depressions, the reduction is expected to be about 70%, since the bending is likely to begin earlier. This stress relaxation occurs even for small induced moments, which are approximately proportional to the depression depth for a given width.

C. The Bauschinger effect on Attenuation of Compressive Yield Threshold

As the vessel pressure is lowered from the peak proof pressure to 0 psi pressure, further bending will occur that changes the curvatures relative to those that are already frozen-in as a result of the pressure build-up and yielding of proof. This bending will superimpose new triangular stress distributions through the liner thickness on top of the residual blunted ones remaining from the peak proof pressures. Depending on the location in the depression, the un-blunted portion that was at a lower tensile stress than the tensile yield stress 128 ksi, may become severely blunted as the vessel pressure is reduced to zero and the liner is put into compression. This blunting occurs even though the nominal or average in-plane compressive stress generated upon unloading to zero pressure is only −80 ksi. The true cause of this premature blunting phenomenon is the Bauschinger effect, whereby the effective yield stress of the liner material when placed into compression, after having suffered a large yield strain in tension, becomes approximately −80 ksi and not −128 ksi as was found in tests performed at NASA Glenn Research Center [1].
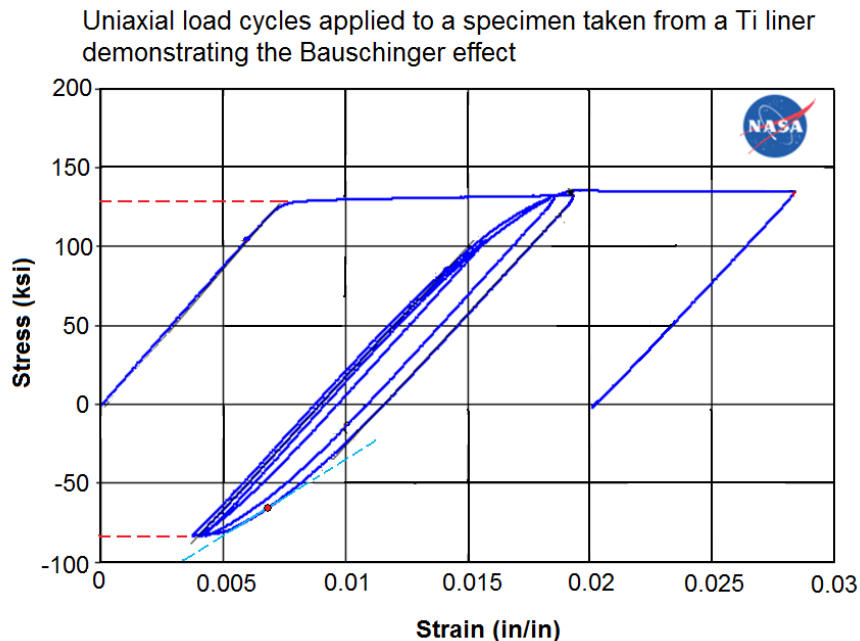

Figure 4. Bauschinger effect in attenuating the compressive yield stress after autofrettage

The most obvious consequence of the Bauschinger effect is a substantially reduced bending moment compared the elastic bending moment associated with such curvature changes from the frozen-in state. The magnitude of the bending moment reduction depends on the details of the bending history and yielding during the void compaction of autofrettage as well as the location in the depression where the bending moment is evaluated. The magnitude of the liner bending moment in the valley area that can safely be sustained at zero vessel pressure is not likely to be much more than 30 percent of the maximum elastic bending moment observed in a simple three-point bending experiment, or about 72 lb-in./in. During depressurization of some vessels, even if the paths of bending moment versus liner in-plane compressive load allow for significantly higher bending moment limits at zero vessel pressure, the Bauschinger effect leads to softening in liner bending response reflected in a moderately reduced secant modulus This will have profound consequences on the potential for liner buckling. We estimate that this will lead to a collapse in interface pressure and thus liner separation from the overwrap. This condition quickly becomes the most critical condition for buckling of the liner.

III. Preliminary Buckling Analysis

To study the formation and effects of a liner depression or valley, initially in terms of liner tension during autofrettage and subsequently in terms of liner compression upon vessel depressurization, we consider an analysis of a plate on an elastic foundation potentially modified to account for spherical curvature effects. We also must consider cylindrical curvature since the depressions are approximately long ellipses in projected outline onto the surface of the sphere as shown in Figures 1 and 2. Thus they are long enough for ring stiffening effects to play some role. We first consider some classic results to frame the problem.

A. Classical Buckling of a Sphere and Simple Correspondence to Plate Buckling

We let E_l be the liner tensile modulus , v_l its Poisson's ratio, t_l be its thickness and R_l be its radius. In the classical theory for buckling of a sphere, the critical external pressure, P_{crit}, and associated critical in-plane (hoop) load , N_{crit}, and buckling half-wavelength, $\lambda_{crit}/2$, are respectively

$$P_{crit} = \frac{2E_l t_l^2}{R_l^2 \sqrt{3(1-v_l^2)}} , \qquad N_{crit} = -\frac{P_{crit}R_l}{2} = -\frac{E_l t_l^2}{R_l\sqrt{3(1-v_l^2)}} , \qquad \lambda_{crit}/2 = \pi\sqrt{R_l t_l}\left(\frac{1}{12(1-v_l^2)}\right)^{1/4} \tag{1}$$

For the liner of the 40-inch Kevlar/epoxy COPV we have $t_l = 0.106$ in., $R_l = 19.19$ in., $E_l = 16.5\times10^6$ psi and $v_l = 0.342$ so for the liner itself under pressure we obtain $P_{crit} = 619$ psi, $N_{crit} = -5,936$ psi and $\lambda_{crit}/2 = 2.50$ in. Thus for the OMS liner alone with no overwrap support, this result predicts collapse of *all* liners at zero vessel pressure, since the interface pressure is about 960 psi, which is well above the calculated 619 psi.

Later we develop the theory for a plate (liner region) on an elastic foundation (the overwrap), but certain results for a simply supported plate are mentioned here. In Euler buckling, the critical, in-plane buckling load, $N_{crit,plate}$, for a simply supported square plate of length and width, *L*, and under biaxial loading is

$$N_{crit,plate} = \frac{\pi^2 E_l t_l^3}{6(1-v_l^2)L^2} \tag{2}$$

Taking the spherical buckling half-wavelength for *L,* i.e., $L = \lambda_{crit}/2$ from (1), yields

$$N_{crit} = \frac{\pi^2 E_l t_l^3}{6(1-v_l^2)}\left/\left[\pi^2 R_l t_l\sqrt{\frac{1}{1 \, 2(1-v_l^2)}}\right]\right. = \frac{E_l t_l^2}{R_l\sqrt{3(1-v^2)}} \tag{3}$$

Surprisingly, the flat-plate plate buckling load is the same as that for the in-plane load of the sphere when its half wavelength is the same as the plate dimension, *L*. This is a key observation, because we can study more complicated buckling of a composite sphere by replacement of critical regions with flat plate sections. In particular we can study the effect of the elastic foundation support of the overwrap on the behavior of the spherical liner.

B. Key Equations for Buckling of a Plate on an Elastic Foundation

The fundamental differential equation for the transverse displacement $v(x)$ of a plate on an elastic foundation in terms of axial distance, x, is the 4th order equation

$$\frac{E_l t_l^3}{12(1-v_l^2)}\frac{d^4v(x)}{dx^4} - N_l \frac{d^2v(x)}{dx^2} + \frac{E_{O,t}}{t_O}v(x) = 0, \quad -\infty < x < \infty \tag{4}$$

where $E_{O,t}$ is the overwrap transverse modulus (through-thickness compressive stiffness), t_O is the overwrap thickness, N_l is the "running" in-plane liner load (with a negative value in compression) and the remaining parameters are as defined in connection with (1). This differential equation for transverse (indentation) displacement, $v(x)$, can be written in terms of a non-dimensional load, N, and stiffness parameter, Φ, as

$$\frac{d^4v}{dx^4} - 2N\frac{d^2v}{dx^2} + \Phi v = 0, \quad -\infty < x < \infty , \qquad N = \frac{6N_l(1-v_l^2)}{E_l t_l^3} , \qquad \Phi = \frac{12E_{O,t}(1-v_l^2)}{E_l t_l^3 t_O} \tag{5}$$

C. Possibility of Reinforcement Effects due to Spherical Shape compared to Flat Plate

Before proceeding, we digress briefly to consider the relative importance of curvature effects associated with the surface contours of the liner depressions, which are roughly elliptical in projected outline on the sphere surface. One might expect the radial curvature along the major axis of the elliptical indentation (approximately the curvature of the liner itself) to act to suppress the simply supported plate buckling along the minor axis (narrow direction of the depression), which will suffer major curvature changes associated with protruding into the inside of the vessel. The theory for cylinder buckling developed by Sam Batdorf can be used to shed light on the importance of this effect. Regarding Batdorf's theory for a short cylindrical shell (with no overwrap support), and with hinged end-conditions, one can derive his results beginning with the liner-only differential equation

$$\frac{E_l t_l^3}{12\left(1-v_l^2\right)}\frac{d^4v}{dx^4} - N_l\frac{d^2v}{dx^2} + \frac{E_l t_l}{R_l^2}v = 0 \tag{6}$$

and adding to this the elastic foundation support effect, which results in

$$\frac{E_l t_l^3}{12\left(1-v_l^2\right)}\frac{d^4v}{dx^4} - N_l\frac{d^2v}{dx^2} + \left(\frac{E_l t_l}{R_l^2} + \frac{E_{O,t}}{t_O}\right)v = 0 \tag{7}$$

In the spirit of obtaining the dimensionless equation (5) we define

$$\breve{\Phi} = \frac{12\left(1-v_l^2\right)}{E_l t_l^3}\left(\frac{E_{O,t}}{t_O} + \frac{E_l t_l}{R_l^2}\right) = \frac{12\left(1-v_l^2\right)E_{O,t}}{E_l t_l^3 t_O}\left(1 + \frac{E_l}{E_{O,t}}\frac{t_l t_O}{R_l^2}\right) \tag{8}$$

For the second stiffness term in parentheses to provide a contribution comparable in magnitude to the first, one would need $E_{O,t} \approx E_l t_l t_O / R_l^2$, and for the 40-inch COPV under study this requires $E_{O,t} \approx 3510\ \mathrm{psi}$, which is much too small (by almost two orders of magnitude as we see later). On the other hand, the natural buckling load, N_l, (with only the cylindrical support) and the natural half-wavelength, $\lambda_{cl}/2$, are found, respectively, to be

$$N_l = -\sqrt{\left(\frac{E_l t_l^3}{3\left(1-v_l^2\right)}\right)\left(\frac{E_l t_l}{R_l^2}\right)} = -\frac{E_l t_l^2}{\sqrt{3\left(1-v_l^2\right)}R_l} = -5,936\ \mathrm{lb/in} \tag{9}$$

and

$$\lambda_{cl}/2 = \frac{\pi}{\sqrt[4]{\breve{\Phi}}} = \pi\sqrt[4]{\frac{E_l t_l^3}{12\left(1-v_l^2\right)}\frac{R_l^2}{E_l t_l}} = \pi\sqrt[4]{\frac{t_l^2 R_l^2}{12\left(1-v_l^2\right)}} = 2.50\ \mathrm{in.} \tag{10}$$

Surprisingly, these are exactly the same results as (2) and (3) for the sphere above. Thus when considering buckling of the liner depressions or indentations, we need only consider plate-like effects in the depressed regions and assess the extent to which overwrap support will suppress buckling or its absence will allow buckling to occur.

We also calculate the buckling half-wavelength for a flat, square, plate-like region (or cylindrical ring) with zero bending moments at each end and free edges on the side (no edges in the ring), and subjected to the in-plane load $N_{l,p=0} = -9,172\ \mathrm{lb/in.}$, the value at 0 psi in the 40 inch COPV. Later we show this is the in-plane liner load at 0 psi vessel pressure. This half-wavelength happens to be the classic Euler result, which for the 40-inch vessel gives

$$\lambda_{eff}/2 = \sqrt{\frac{\pi^2 E_l t_l^3}{6\left(1-v_l^2\right)N_{l,p=0}}} = 2.00\ \mathrm{in.} \tag{11}$$

This establishes a critical length-scale of 2.0 inches between zero bending moment points acting as hinges. If such lengths exceed 2.0 inches, buckling becomes a risk particularly if the overwrap support becomes ineffective once the interface pressure falls to zero, indicating the onset of liner separation from the overwrap.

IV. More Detailed Buckling Analysis

Next we consider a more detailed analysis, considering both the pressurization stage during autofrettage when overwrap compaction and through-thickness stiffness increase occurs, and liner yielding and indentation occurs from tow and band cross-over pile-ups. Then we consider the depressurization phase where further liner yielding and depressurization may occur if the indentation is sufficiently deep. First we present the solution to the main

differential equation (5) subject to the boundary conditions associated with an imposed displacement, δ_b, or equivalent load along a line perpendicular the in-plane load, N, and an imposed zero slope along that line. (The case of non-zero slope has also been solved but is not presented.)

The solution begins with the usual complex exponential form for such equations, namely, $v = Ce^{sx}$, which yields the characteristic equation, $s^4 - 2Ns^2 + \Phi = 0$, which has the squared roots

$$s^2 = N \pm \begin{cases} i\sqrt{\Phi - N^2}, & \Phi > N^2 \\ \sqrt{N^2 - \Phi}, & N^2 > \Phi \end{cases} \tag{12}$$

A. Liner in In-Plane Tension.

When N is positive and the liner is in tension, we could have the second case where s^2 is real provided N is sufficiently large. However this condition requires $N > \sqrt{\Phi}$, and for $E_{O,t} = 250,000$ psi in the compacted state

$$N_l > \sqrt{\left(\frac{E_l t_l^3}{3(1 - v_l^2)}\right)\left(\frac{E_{O,t}}{t_O}\right)} = 50,100 \text{ lb/in} \tag{13}$$

but for the 40-inch vessel, the maximum value for N_l in tension is the liner yield value, $N_{l,y} = \sigma_{l,y} t_l = 13,568$ lb/in, so s^2 cannot be real. This means that the disturbance due to overwrap protrusion will have a decaying sinusoidal character with mild overshoots (rather than pure exponential decay). This is consistent with the profilometry results described earlier. Thus we need only consider the case $\Phi > N^2$ and this separated into two sub-cases

$$N = \begin{cases} N, & N > 0 \quad \text{(liner in tension)} \\ -|N|, & N < 0 \quad \text{(liner in compression)} \end{cases} \tag{14}$$

The case of loading in tension is important to the formation of the disturbance shape during autofrettage ($N > 0$ and $\Phi - N^2$). In this case characteristic equation $s^4 - 2Ns^2 + \Phi = 0$ factors as

$$\left(s^2 - \sqrt{\Phi}e^{+i\theta}\right)\left(s^2 - \sqrt{\Phi}e^{-i\theta}\right) = \left(s + \sqrt[4]{\Phi}e^{+i\theta/2}\right)\left(s - \sqrt[4]{\Phi}e^{+i\theta/2}\right)\left(s + \sqrt[4]{\Phi}e^{-i\theta/2}\right)\left(s + \sqrt[4]{\Phi}e^{-i\theta/2}\right) = 0 \tag{15}$$

where $\tan\theta = \sqrt{(\Phi - N^2)/N^2}$, thus yielding four roots, s_1, s_2, s_3 and s_4 given by

$$s_{1,2} = \sqrt[4]{\Phi}\left(\cos(\theta/2) \pm i\sin(\theta/2)\right), \qquad s_{3,4} = -\sqrt[4]{\Phi}\left(\cos(\theta/2) \pm i\sin(\theta/2)\right) \tag{16}$$

Since $\tan^2\theta + 1 = 1/\cos^2\theta$ we obtain $\cos\theta = 2\cos^2(\theta/2) - 1 = 1 - 2\sin^2(\theta/2) = 1 - N/\sqrt{\Phi}$ so that

$$\cos(\theta/2) = \sqrt{\frac{1 + \cos\theta}{2}} = \sqrt{\frac{\sqrt{\Phi} + N}{2\sqrt{\Phi}}}, \quad \sin(\theta/2) = \sqrt{\frac{1 - \cos\theta}{2}} = \sqrt{\frac{\sqrt{\Phi} - N}{2\sqrt{\Phi}}} \tag{17}$$

Thus we have the general solution form

$$v(x) = C_1 e^{-\sqrt[4]{\Phi}\cos(\theta/2)x}\cos\left(\sqrt[4]{\Phi}\sin(\theta/2)x\right) + C_2 e^{-\sqrt[4]{\Phi}\sin(\theta/2)x}\sin\left(\sqrt[4]{\Phi}\sin(\theta/2)x\right)$$
$$+ C_3 e^{\sqrt[4]{\Phi}\cos(\theta/2)x}\cos\left(\sqrt[4]{\Phi}\sin(\theta/2)x\right) + C_4 e^{\sqrt[4]{\Phi}\sin(\theta/2)x}\sin\left(\sqrt[4]{\Phi}\sin(\theta/2)x\right) \tag{18}$$

which applies separately on each side of the line displacement(load) which we place at $x = 0$. There can be no unbounded solutions as $x \to \pm\infty$ so that $C_3 = C_4 = 0$ for $x > 0$, and $C_1 = C_2 = 0$ for $x < 0$.

For the boundary conditions we prescribe a displacement and slope, respectively, as $v(0) = -\delta_b$ and $dv(0)/dx = 0$. Using absolute value functions in x as well as symmetry and continuity, we obtain the displacement, slope and curvature, respectively, as

$$v(x) = -\delta_b e^{-\sqrt[4]{\Phi}\cos(\theta/2)|x|}\left\{\cos\left(\sqrt[4]{\Phi}\sin(\theta/2)x\right) + \cot(\theta/2)\ \sin\left(\sqrt[4]{\Phi}\sin(\theta/2)|x|\right)\right\}, \quad -\infty < x < \infty \tag{19}$$

$$\frac{dv(x)}{dx} = \delta_b \frac{\sqrt[4]{\Phi}}{\sin(\theta/2)} e^{-\sqrt[4]{\Phi}\cos(\theta/2)|x|} \sin\left(\sqrt[4]{\Phi}\sin(\theta/2)x\right), \quad -\infty < x < \infty \tag{20}$$

and

$$\frac{dv^2(x)}{dx^2} = \delta_b \sqrt[2]{\Phi} e^{-\sqrt[4]{\Phi}\cos(\theta/2)|x|}\left\{\cos\left(\sqrt[4]{\Phi}\sin(\theta/2)x\right) - \cot(\theta/2)\sin\left(\sqrt[4]{\Phi}\sin(\theta/2)|x|\right)\right\}, \quad -\infty < x < \infty \tag{21}$$

The depression shape half wavelength is computed by noting that the frequency of the oscillation is $f = \sqrt[4]{\Phi}\sin(\theta/2)/(2\pi)$ and the half-wavelength is thus

$$\lambda_{dep}/2 = \frac{\pi}{\sqrt[4]{\Phi}\sin(\theta/2)} \tag{22}$$

This is the "decay" oscillation wavelength of the depression, and it might be matched to profilometer zero crossing points of displacements. However this is misleading since in studying experimental profiles one should really consider the locations of the zeros of $v(x)$ in order to determine points relevant to characteristic lengths. In (19) we note that for $x > 0$, the zero crossing for $x > 0$ actually occurs at $\sqrt[4]{\Phi}\sin(\theta/2)x + \theta/2 = \pi$ so that an effective half-wavelength (width of the valley) might be measured as double this length, or

$$\lambda_{d,eff}/2 = \frac{2\pi - \theta}{\sqrt[4]{\Phi}\sin(\theta/2)} \tag{23}$$

From the second derivative or curvature once can calculate the points, $x = \pm x_{m,0}$, of zero bending moment. From (21), these can be shown to be $x_{m,0} = \pm(\theta/2)/\left(\sqrt[4]{\Phi}\sin(\theta/2)\right)$. The key point is that the zero points for the bending moment are very different from those of the displacement itself. The total length equivalent to an *effective characteristic buckling half-wavelength*, associated with the first point of zero bending moment on each side, is double the above value in (24) or

$$\lambda_{m,0}/2 = \frac{\theta}{\sqrt[4]{\Phi}\sin(\theta/2)} \tag{24}$$

Also, this length is different from the width of the valley itself, (23), or the mathematical wavelength, (22). This means that modeling the depression as a half-cosine wave with half-wavelength $\lambda_{d,eff}/2$ or even $\lambda_{dep}/2$ can lead to errors in the bending moment zero points thus missing the possibility of the depression turning into a buckle if separation begins to occur at the interface.

B. Liner in In-Plane Compression at Zero Vessel Pressure

The solution approach in this case is similar to the case in liner tension just treated. For the boundary condition $\gamma_b = 0$, $\delta_b \neq 0$, the displacement, slope and curvature are respectively

$$v(x) = -\delta_b \frac{e^{-\sqrt[4]{\Phi}\sin(\theta/2)|x|}}{\cos(\theta/2)} \cos\left(\sqrt[4]{\Phi}\cos(\theta/2)|x| - \theta/2\right), \quad -\infty < x < \infty \tag{25}$$

$$\frac{dv(x)}{dx} = \delta_b \frac{\sqrt[4]{\Phi}}{\cos(\theta/2)} e^{-\sqrt[4]{\Phi}\sin(\theta/2)|x|} \sin\left(\sqrt[4]{\Phi}\cos(\theta/2)x\right), -\infty < x < \infty \tag{26}$$

and

$$\frac{dv^2(x)}{dx^2} = \delta_b \frac{\sqrt[2]{\Phi}e^{-\sqrt[4]{\Phi}\sin(\theta/2)|x|}}{\cos(\theta/2)} \cos\left(\sqrt[4]{\Phi}\cos(\theta/2)x + \theta/2\right), \quad -\infty < x < \infty \tag{27}$$

Here we note that the mathematical half wavelength of the depression decay is

$$\lambda_{dep}/2 = \frac{\pi}{\sqrt[4]{\Phi}\cos(\theta/2)} \tag{28}$$

The effective half-wavelength based on the zero-crossings of the displacement, $v(x)$, is

$$\lambda_{d,eff}/2 = \frac{\theta + \pi}{\sqrt[4]{\Phi}\cos(\theta/2)} \tag{29}$$

and for the zero bending moment location an effective half-wavelength is

$$\lambda_{m,0}/2 = \frac{\pi - \theta}{\sqrt[4]{\Phi}\cos(\theta/2)} \tag{30}$$

Again this apparent half-wavelength resulting in buckling concern will be much smaller than the apparent half-wavelength of the waveform itself given by (28).

C. Analysis of Indentation and Deformation during Overwrap Compaction Developed During Autofrettage

In addition to the frozen-in displacements due to autofrettage, there is a frozen-in bending moment distribution, which is *not* proportional to the second derivative of the frozen in displacement, because plastic yielding of the liner occurs during autofrettage that greatly reduces this moment especially at the point of largest curvature at the deepest part of the liner depression. The process of generating the frozen-in displacement profile comes mainly from void compaction when the liner is in substantial tension and the liner overwrap interface pressure is elevated because of the high proof pressure. The relevant tension, $N_{l,c}$, may be less than the peak value during autofrettage, denoted as $N_{l,p}$. Pressure versus boss-to-boss displacement records and experiments on overwrap sections show that much of this compaction occurs well before the liner tension reaches $N_{l,p}$, thus it is appropriate to consider the sensitivity of the results to any differences between $N_{l,c}$ and $N_{l,p}$.

Regarding the frozen-in, bending moment distribution, since the peak vessel pressure during the proof hold of autofrettage (about 6520 psi in a 40 inch vessel) is much higher than the point where yielding begins (beyond which $N_l = N_{l,p}$), the plastic yield strain at the end of the proof hold is more than double the elastic strain when yielding begins (at about 3200 psi to 3400 psi). Thus the bending moments at the peak proof pressure will be less than half the values calculated on the basis of bending of a purely elastic liner (ignoring yielding), and if the depression is sufficiently deep, the peak bending moment is reduced to about 30% of the nominal elastic value. However, the bending moment distribution at this point, where $N_l = N_{l,p}$, is different from what it becomes at the reference point $N_l = 0$, passed through during depressurization. Likewise, the associated distribution of liner-overwrap interface pressure is also different and some care is necessary to distinguish between them.

We begin by calculating the bending moment distribution and associated interface pressure distribution at the peak proof pressure point where $N_l = N_{l,p}$ and the peak displacement is $-\delta_{b,p}$. We then follow the unloading process from the peak point down to the reference state, $N_l = 0$ (at ~ 2650 psi). This will allow us to compare displacements and arrive at an appropriate reference displacement, $-\delta_{b,p}$. Once this has been accomplished, we can follow the various deformation components, bending moments and interface pressures all the way from the maximum tension at autofrettage $N_l = N_{l,p}$, down through the point of zero tension, $N_l = 0$ on vessel depressurization to the maximum compression at 0 psi vessel pressure, $N_l = -N_{l,u}$.

After winding and curing, and before autofrettage begins, the liner surface is flat and there is no interface pressure at all (except for a small effect of the winding tension). However as the autofrettage process begins and the vessel pressure is increased from 0 psi, compaction occurs in the overwrap. The effect on the liner displacement relative to an equilibrium state (whereby the liner radius increases on average as it physically expands into the overwrap) can be viewed as a local depression in the liner that develops relative to this equilibrium state around a line perpendicular to the in-plane tensile load. This depression can be viewed as the disturbance that results from a very narrow, but very stiff region of the overwrap with many fewer voids and which undergoes very little compaction. The physical cause is likely the result of sudden overlap of the edges of two adjacent bands in the same wrap pattern as they proceed from the equator to the boss. In general overlap must occur in virtually all bands of a wrap pattern as the circumference, at increasing latitude, decreases relative to that at the equator, such that the bands can no longer lie beside each other in parallel. Each band must therefore jump and cross over the band laid down just before it. This is the cause of the rippling effect seen in Figures 1 and 2. However each wrap pattern must have a starting point, and the first band laid down will have a different overlap circumstance since it must, in fact, be flat

everywhere since there is no previous band for it cross over. Note that at bands are stacked four deep since each wrap pattern has two passes around the vessel of $360°$ each and full coverage of the vessel occurs with just $180°$ degrees of a pass. The result is that, the total stacking of tows in the bands at the beginning and end of a wrap pattern and at some latitude location, may be two higher than on average around the rest of the vessel. This will cause a local bump in the overwrap and consequently a depression in the liner.

To capture the effects of this phenomenon, the non-dimensional differential equation describing the transverse liner deformation from an equilibrium position is nominally given by

$$\frac{d^4 v_p}{dx^4} - 2N_p \frac{d^2 v_p}{dx^2} + \Phi_p v_p = 0, \quad -\infty < x < \infty, \quad N_p = \frac{6N_{l,p}\left(1-v_l^2\right)}{E_l t_l^3}, \quad \Phi_p = \frac{12E_{O,t,0}\left(1-v_l^2\right)}{E_l t_l^3 t_O} \tag{31}$$

The relevant transverse stiffness of the overwrap for forming the depression shape is the low value $E_{O,t,0}$ and not $E_{O,t}$, which applies during depressurization after full overwrap compaction and the transverse stiffness is about 10 times larger. Also the tension is taken as $N_{l,p}$ rather than $N_{l,c}$ since the effects of any differences are small.

As the autofrettage process proceeds with increasing vessel pressure, a local depression develops in the liner around a line perpendicular to the in plane tensile load. This depression can be viewed as being caused by a displacement imposed along a line caused by a corresponding line force from an infinitesimally narrow, region that undergoes very little compaction compared to elsewhere in the overwrap during the pressure buildup of autofrettage. The effect is nominally captured through the boundary conditions

$$v_p(0) = -\delta_{b,p}, \quad \lim_{|x|\to 0} \frac{dv_p(x)}{dx} = 0, \quad \lim_{|x|\to\infty} v_p(x) = 0 \tag{32}$$

where $\delta_{b,p}$ is the depression depth that finally results at the peak proof pressure when $N_l = N_{l,p}$.
The solution to (31) and (32), determined earlier in slightly different notation, can be written as

$$v_p(x) = -\delta_{b,p} e^{-\omega_0 \varphi_0 |x|} \left\{ \cos(\omega_0 x) + \varphi_0 \sin(\omega_0 |x|) \right\}, \quad -\infty < x < \infty \tag{33}$$

where in the present case

$$\omega_0 = \sqrt[4]{\Phi_p} \sin(\theta_0/2), \quad \cos(\theta_0/2) = \sqrt{\frac{\sqrt{\Phi_p} + N_p}{2\sqrt{\Phi_p}}}, \quad \sin(\theta_0/2) = \sqrt{\frac{\sqrt{\Phi_p} - N_p}{2\sqrt{\Phi_p}}}, \quad \varphi_0 = \sqrt{\frac{\sqrt{\Phi_p} + N_p}{\sqrt{\Phi_p} - N_p}} \tag{34}$$

Also several useful identities can be demonstrated, namely

$$\sin^2(\theta_0/2) = \frac{1}{\varphi_0^2 + 1}, \quad \cos^2(\theta_0/2) = \frac{\varphi_0^2}{\varphi_0^2 + 1}, \quad \Phi_p = \omega_0^4\left(1+\varphi_0^2\right)^2, \quad N_p = \omega_0^2\left(\varphi_0^2 - 1\right) \tag{35}$$

Thus the solution to the governing differential equation (31) and its four derivatives reduce to

$$v_p(x) = -\delta_{b,p} e^{-\omega_0 \varphi_0 |x|} \left\{ \cos(\omega_0 x) + \varphi_0 \sin(\omega_0 |x|) \right\}, \quad -\infty < x < \infty \tag{36}$$

$$\frac{dv_p(x)}{dx} = \text{sgn}(x)\delta_{b,p}\omega_0\left(1+\varphi_0^2\right)e^{-\omega_0 \varphi_0 |x|} \sin(\omega_0 |x|), \quad -\infty < x < \infty \tag{37}$$

$$\frac{d^2 v_p(x)}{dx^2} = \delta_{b,p}\omega_0^2\left(1+\varphi_0^2\right)e^{-\omega_0 \varphi_0 |x|} \left\{ \cos(\omega_0 x) - \varphi_0 \sin(\omega_0 |x|) \right\}, \quad -\infty < x < \infty \tag{38}$$

$$\frac{d^3 v_p(x)}{dx^3} = -\text{sgn}(x)2\delta_{b,p}\omega_0^3\varphi_0\left(1+\varphi_0^2\right)e^{-\omega_0 \varphi_0 |x|} \left\{ \cos(\omega_0 x) + \frac{1-\varphi_0^2}{2\varphi_0}\sin(\omega_0 |x|) \right\} \tag{39}$$

and

$$\begin{aligned}
\frac{d^4 v_p(x)}{dx^4} &= -4\delta_{b,p}\omega_0^3\varphi_0\left(1+\varphi_0^2\right)\delta(x) + \delta_{b,p}\Phi_p e^{-\omega_0 \varphi_0 |x|}\left\{\cos(\omega_0 x) + \varphi_0 \sin(\omega_0 |x|)\right\} \\
&\quad + 2\delta_{b,p}\omega_0^2\left(1+\varphi_0^2\right)\omega_0^2\left(\varphi_0^2 - 1\right)e^{-\omega_0 \varphi_0 |x|}\left\{\cos(\omega_0 x) - \varphi_0 \sin(\omega_0 |x|)\right\} \\
&= -4\delta_{b,p}\omega_0^3\varphi_0\left(1+\varphi_0^2\right)\delta(x) - \Phi_0 v_p(x) + 2N_p \frac{d^2 v_p(x)}{dx^2}
\end{aligned} \tag{40}$$

where $\delta(x)$ is the Dirac delta function. Thus the governing differential equation for studying the depression nominal characteristics becomes

$$\frac{d^4 v_p(x)}{dx^4} - 2N_p \frac{d^2 v_p(x)}{dx^2} + \Phi_p v_p(x) = -4\delta_{b,p}\omega_0^3 \varphi_0 \left(1+\varphi_0^2\right)\delta(x), \quad -\infty < x < \infty \tag{41}$$

subject to no other boundary conditions other than $v_p(x) \to 0$, $|x| \to \infty$. As stated this is a nominal solution, but modifications are required to obtain a more realistic description that accounts for the dispersive effects of liner yielding during the peak tension of autofrettage.

D. Residual Bending Moments and Spring-Back Pressures at the Liner-Overwrap Interface.

As the peak pressure of autofrettage is approached, liner yielding takes place that relieves much of the bending moment and resulting stress in the liner in the depression region. This means that the pressure distribution will be more dispersed than reflected by the concentrated scaled line force, $-4\delta_{b,p}\omega_0^3\varphi_0\left(1+\varphi_0^2\right)\delta(x)$, on the right-hand side of (41). Nonetheless a significant residual bending moment will remain and can be viewed as generating a spring-back force that is manifest as an interface pressure disturbance relative to the nominally uniform interface pressure over the liner-overwrap interface. We assume this liner yielding limits the maximum obtainable bending moment at the peak deflection to $M_{pf,\max} = K_{pf,\max} M_{e,\max}$ where $M_{e,\max}$ is the maximum elastic bending moment (beyond which plastic yielding occurs) one would obtain in a simple three-point bending experiment, and $0 < K_{pf,\max} < 1$ is the fraction that would remain if the specimen were subsequently (while maintaining its bent shape) strained in tension to some value more than twice (about 2.2 times) the uniaxial yield strain. A reasonable value is $K_{pf,\max} \approx 0.3$. Beyond some distance away from this peak, say $|x| > |\hat{x}|$, we assume the yielding generally lowers the bending moment to a value K_p times the nominally induced value, where $K_p \approx 0.45$. However, within the region close to the peak, denoted $-|\hat{x}| < x < |\hat{x}|$, we assume the bending moment is driven by the form of the local but somewhat relaxed and diffused pressure distribution around the original line load (or displacement). This local pressure distribution, denoted, $p_p(x)$, will be taken to be parabolic (2nd order polynomial) with 4th order edge terms to provide continuity and a smooth first derivative at the transition points $x = \pm|\hat{x}|$. This pressure disturbance will integrate twice to result in a 6th order polynomial for the bending moment profile over the region $-|\hat{x}| < x < |\hat{x}|$, but will actually be dominated by a 2nd order parabola rather than the triangular peak in (38) resulting from the line load (as naturally occurs in three point bending), which nulls out. The resulting displacement, which requires two more integrations, is virtually indistinguishable from the displacement given by (36). However, the details are important in determining an accurate description of the pressure distribution, which is critical for determining the possibility of liner separation from the overwrap triggering buckling, as the vessel pressure decreases to zero and the liner is forced into in-plane (hoop-type) compression.

We begin with the original form of the equation under the concentrated line load, whereby the overall interface pressure profile is obtained from (40) and (35) as

$$p_{line}(x) = F_p(x) + K_p EI \delta_{b,p}\omega_0^4 \left(1+\varphi_0^2\right)^2 e^{-\omega_0\varphi_0|x|}\left\{\cos(\omega_0 x) + \varphi_0 \sin(\omega_0 |x|)\right\}, \quad -\infty < x < \infty \tag{42}$$

where the flexural rigidity, line load, and a convenient line-load like quantity (force per unit length) are given by

$$EI = \frac{E_l t_l^3}{12\left(1-v_l^2\right)}, \quad F_p(x) = -K_p EI 4\delta_{b,p}\omega_0^3\varphi_0\left(1+\varphi_0^2\right)\delta(x) \quad \text{and} \quad \hat{F}_p = K_p EI 4\delta_{b,p}\omega_0^3\varphi_0\left(1+\varphi_0^2\right) \tag{43}$$

Thus the local pressure distribution is

$$p_p(x) = -\hat{F}_p\delta(x) + \frac{\hat{F}_p\omega_0\left(1+\varphi_0^2\right)}{4\varphi_0}e^{-\omega_0\varphi_0|x|}\left\{\cos(\omega_0 x) + \varphi_0 \sin(\omega_0 |x|)\right\}, \quad -\infty < x < \infty \tag{44}$$

Due to the effects of yield relaxation and compaction, we assume the line load $-\hat{F}_p\delta(x)$ becomes diffused and can be replaced by the pressure profile described by the 4th order polynomial

$$\hat{p}_p(x) = -p_{max}\left(1 - A(x/\hat{x})^2 + B(x/\hat{x})^4\right), \quad -\hat{x} < x < \hat{x} \tag{45}$$

where $(-\hat{x}, \hat{x})$ is the zone over which the $\hat{p}_p(x)$ acts. We assume that both the magnitude of the pressure and the slope are zero along the transition lines $x = \pm\hat{x}$, that is, $\hat{p}_p(\pm\hat{x}) = d\hat{p}_p(\hat{x})/dx\big|_{x=\pm\hat{x}} = 0$. These two equations result in

$$\hat{p}_p(x) = -p_{max}\left(1 - 2(x/\hat{x})^2 + (x/\hat{x})^4\right) \tag{46}$$

Also, we require force balance with respect to the original line load so that $\int_{-\hat{x}}^{\hat{x}} \hat{p}_p(x)dx = -\hat{F}_p$ from which we get $p_{max} = (15/8)\hat{F}_p/(2\hat{x})$ and thus the diffused local pressure profile is

$$\hat{p}_p(x) = \begin{cases} -\left(\dfrac{15}{8}\right)\dfrac{\hat{F}_p}{2\hat{x}}\left[1 - 2(x/\hat{x})^2 + (x/\hat{x})^4\right], & -\hat{x} < x < x \\ 0, & -\infty < x < -\hat{x} \text{ or } \hat{x} < x < \infty \end{cases} \tag{47}$$

and overall the pressure profile is

$$p_p(x) = \hat{p}_p(x) + \left(\hat{F}_p\omega_0(\varphi_0^2 + 1)/(4\varphi_0)\right)e^{-\omega_0\varphi_0|x|}\left\{\cos(\omega_0 x) + \varphi_0\sin(\omega_0|x|)\right\}, \quad -\infty < x < \infty, \tag{48}$$

Next we consider the shear profile around $\hat{x} = 0$ and first calculate the shear distribution from the local distributed pressure $\hat{p}_p(x)$ over $-\hat{x} < x < \hat{x}$. This is $\hat{S}_p(x) = -\int_0^x \hat{p}_p(\eta)d\eta$ which yields

$$\hat{S}_p(x) = -\left(\frac{15}{8}\right)\frac{\hat{F}_p}{2}\left(\frac{x}{\hat{x}} - \frac{2}{3}\left(\frac{x}{\hat{x}}\right)^3 + \frac{1}{5}\left(\frac{x}{\hat{x}}\right)^5\right) \quad \text{and} \quad \hat{S}_p(\hat{x}) - \hat{S}_p(-\hat{x}) = -\hat{F}_p \tag{49}$$

Calculating the total shear profile in the beam requires care. We know that for the line load, the shear profile is

$$S_{line}(x) = K_p EI \frac{d^3 v_p(x)}{dx^3} = -\text{sgn}(x)\frac{\hat{F}_p}{2}e^{-\omega_0\varphi_0|x|}\left\{\cos(\omega_0 x) - \frac{\varphi_0^2 - 1}{2\varphi_0}\sin(\omega_0|x|)\right\}, \quad -\infty < x < \infty \tag{50}$$

where a jump of magnitude $2(\hat{F}_p/2) = \hat{F}_p$ occurs at $x = 0$. For the distributed version of the load the overall decrease of magnitude $\hat{F}_p$ occurs more gradually over $-\hat{x} < x < \hat{x}$, which is accomplished by way of

$$S_p(x) = \begin{cases} -\text{sgn}(x)\dfrac{\hat{F}_p}{2}e^{-\omega_0|x|}\left\{\cos(\omega_0 x) - \dfrac{\varphi_0^2 - 1}{2\varphi_0}\sin(\omega_0|x|)\right\}, & \hat{x} < |x| < \infty \\ -\text{sgn}(x)\dfrac{\hat{F}_p}{2}e^{-\omega_0|x|}\left\{\cos(\omega_0 x) - \dfrac{\varphi_0^2 - 1}{2\varphi_0}\sin(\omega_0|x|) - 1\right\} + \hat{S}_p(x), & 0 < |x| < \hat{x} \end{cases} \tag{51}$$

This profile and its derivative are both continuous so the pressure profile is also continuous as was initially assumed.

To obtain the moment distribution, we note that $M_p(x) = K_p EI \, d^2 v_p(x)/dx^2 = \int_{-\infty}^x S_p(x)dx$ and adapting the results for a line load given earlier, whereby we obtain

$$M_{line}(x) = K_p EI \, d^2 v_p(x)/dx^2 = \left(\hat{F}_p/(4\omega_0\varphi_0)\right)e^{-\omega_0\varphi_0|x|}\left\{\cos(\omega_0 x) - \varphi_0\sin(\omega_0|x|)\right\}, \quad -\infty < x < \infty \tag{52}$$

we find that

$$M_p(x) = \begin{cases} \dfrac{\hat{F}_p}{4\omega_0\varphi_0}e^{-\omega_0\varphi_0|x|}\left\{\cos(\omega_0 x) - \varphi_0\sin(\omega_0|x|)\right\}, & \hat{x} < |x| < \infty \\ \hat{M}_p(x) + \dfrac{\hat{F}_p}{4\omega_0\varphi_0}e^{-\omega_0\varphi_0|x|}\left\{\cos(\omega_0 x) - \varphi_0\sin(\omega_0|x|)\right\}, & 0 < |x| < \hat{x} \end{cases} \tag{53}$$

whereby

$$\hat{M}_p(x) = \int_{-\hat{x}}^{x} \hat{S}_p(x)\,dv + \mathrm{sgn}(x)\frac{\hat{F}_p}{2}\int_{-\hat{x}}^{x} 1\,dv$$

$$= \frac{\hat{F}_p}{4\varphi_0\omega_0}(\varphi_0\omega_0\hat{x})\left\{\frac{15}{4}\left(\frac{1}{2}\left[1-\left(\frac{x}{\hat{x}}\right)^2\right]-\frac{1}{6}\left[1-\left(\frac{x}{\hat{x}}\right)^4\right]+\frac{1}{3}\left[1-\left(\frac{x}{\hat{x}}\right)^6\right]\right)\Big|_0 - 2\frac{\hat{x}-|x|}{\hat{x}}\right\} \qquad (54)$$

Note that $M_p(0)$ reduces to

$$M_p(0) = \frac{\hat{F}_p}{4\omega_0\varphi_0}\left(1-\frac{5}{8}(\omega_0\varphi_0\hat{x})\right) \qquad (55)$$

However, we limit $\left|\hat{M}_p(0)\right|$ to the maximum value $M_{pf,\max}$ and this allows us to solve for $\hat{x}$ using (54)) yielding

$$\hat{x} = \frac{8}{5\omega_0\varphi_0}\left(1-\frac{M_{pf,\max}\,4\omega_0\varphi_0}{\hat{F}_0}\right) \qquad (56)$$

E. Deformation during Depressurization due to the Frozen-in Depression Occurring during Autofrettage.

Here we develop an analysis of deformation and potential buckling of a plate on an elastic foundation as a result of a frozen-in, transient wave disturbance that has occurred autofrettage and is characterized by behavior at the peak proof pressure and maximum liner tension. This disturbance is residual deformation induced from a sharp bump from fabrication (band crossovers and tow pileups), but modified by overwrap compaction and plastic yielding in the liner. Earlier we considered the effects of a residual bending moment and associated disturbance in interface pressure also with reference to the peak proof pressure and associated maximum liner tension. On depressurization of the vessel the newly induced disturbance from the compressive load in the liner may have a characteristic wavelength that is different from the one induced by the original sharp disturbance during pressurization and the bending wavelengths may be much longer and different in shape from the frozen in shape. The main cause is the greatly increased transverse or through-thickness stiffness of the overwrap from void compaction. In this subsection we derive a mathematical description of the behavior on depressurization.

We let the initial, frozen-in, transverse displacement be of the form

$$v_0(x) = -\delta_{b,0}e^{-\omega_0\varphi_0|x|}\left\{\cos(\omega_0 x)+\varphi_0\sin(\omega_0|x|)\right\}, \quad -\infty < x < \infty \qquad (57)$$

where $\delta_{b,0}$ is the frozen in displacement corresponding to a reference state with zero liner tension, and ω_0 and φ_0, with subscripts '0' given by (34), are waveform parameters associated with the initial, frozen-in, geometry, which were appropriate during the pressurization. The displacement parameter here is taken as $\delta_{b,0}$ since the reference liner tension state is different from that for $\delta_{b,p}$ at the proof peak, though their magnitudes are nearly the same.

Note that the original model parameters without subscripts, Φ, N, were defined in (5) in terms of geometry and mechanical properties of the plate and elastic support of the overwrap and are used now to refer to the *depressurization* phase of the vessel since the relevant through-thickness stiffness of the overwrap is $E_{O,t}$, the high stiffness of the compacted state. The parameters N_p and Φ_p in (31) were used to refer to the tension phase during autofrettage where the eventual "frozen-in" profile was generated under the low overwrap through-thickness stiffness, $E_{O,t,0}$, prior to compaction. Thus $N_{l,0}$ is in-plane, tensile liner load appropriate to the autofrettage phase at peak pressure and N_l, a variable, is in-plane liner compressive load upon depressurization after autofrettage. Thus the basic model parameters without subscripts are given in (5) and with subscripts are

$$N_0 = \frac{6N_{l,0}}{E_l t_l^3}, \quad \text{and} \quad \Phi_0 = \frac{12(1-\nu_l^2)E_{O,t,0}}{E_l t_l^3 t_O} = \Phi_p \qquad (58)$$

Also

$$\cos(\theta_0/2) = \sqrt{\frac{\sqrt{\Phi_0}-N_0}{2\sqrt{\Phi_0}}}, \quad \sin(\theta_0/2) = \sqrt{\frac{\sqrt{\Phi_0}+N_0}{2\sqrt{\Phi_0}}}, \quad \omega_0 = \sqrt[4]{\Phi_0}\cos(\theta_0/2) \text{ and } \varphi_0 = \tan(\theta_0/2) \qquad (59)$$

and appreciate that $E_{O,t,0} \ll E_{O,t}$ after overwrap compaction, the difference being up to an order of magnitude.

We let the total transverse displacement, v, be the sum of the incremental displacement, $\tilde{v}$, induced by the scaled applied axial load, N, and the 'frozen-in' displacement, v_0, i.e., $v(x) = \tilde{v}(x) + v_0(x)$ so that

$$\tilde{v}(x) = v(x) - v_0(x) \tag{60}$$

is the transverse displacement difference caused by the loading. On depressurization, the differential equation for the transverse displacement of a plate section of the liner and overwrap is the 4th order equation

$$\frac{d^4\tilde{v}}{dx^4} - 2N\frac{d^2v}{dx^2} + \Phi\tilde{v} = 0, \quad -\infty < x < \infty \tag{61}$$

Note that the moment of the applied axial load depends on the *total* displacement (hence no 'over-tilde' on the second derivative), whereas the transverse displacement and bending components depend on the displacement increment. From (60) we can write (61) as

$$\frac{d^4\tilde{v}}{dx^4} - 2N\frac{d^2\tilde{v}}{dx^2} + \Phi\tilde{v} = 2N\frac{d^2v_0}{dx^2}, \quad -\infty < x < \infty \tag{62}$$

where the boundary conditions now are $\tilde{v}(x) \to 0$ as $x \to \pm\infty$ and $d\tilde{v}(0)/dx = d^3\tilde{v}(0)/dx^3 = 0$ and we note that $\tilde{v}(x) = 0$, $-\infty < x < \infty$ when N = 0. In terms of the actual displacements, $v(x)$, the key differential equation is

$$\frac{d^4v}{dx^4} - 2N\frac{d^2v}{dx^2} + \Phi v = \frac{d^4v_0}{dx^4} + \Phi v_0, \quad -\infty < x < \infty \tag{63}$$

where the boundary conditions become $v(x) \to 0$ as $x \to \pm\infty$, and $dv(0)/dx = d^3v(0)/dx^3 = 0$. However, it is simpler to solve the problem in terms of the incremental disturbance upon unloading, $\tilde{v}$, and then to add the initial frozen-in disturbance, v_0, to get the final result, $v(x) = v_0(x) + \tilde{v}(x)$.

We will need several derivatives of the initial displacement profile (57) to solve the problem. We consider the case, $x > 0$ and from symmetry arguments construct the full solution for $-\infty < x < \infty$. Thus from (57) we have

$$\frac{dv_0}{dx} = \delta_{b,0}\omega_0\left(\varphi_0^2 + 1\right)e^{-\omega_0\varphi_0 x}\sin(\omega_0 x), \quad x > 0 \tag{64}$$

$$\frac{d^2v_0}{dx^2} = \delta_{b,0}\omega_0^2\left(\varphi_0^2 + 1\right)e^{-\omega_0\varphi_0 x}\left\{\cos(\omega_0 x) - \varphi_0\sin(\omega_0 x)\right\}, \quad x > 0 \tag{65}$$

$$\frac{d^3v_0}{dx^3} = \delta_{b,0}\omega_0^3\left(\varphi_0^2 + 1\right)e^{-\omega_0\varphi_0 x}\left\{\left(\varphi_0^2 - 1\right)\sin(\omega_0 x) - 2\varphi_0\cos(\omega_0 x)\right\}, \quad x > 0 \tag{66}$$

and

$$\frac{d^4v_0}{dx^4} = \delta_{b,0}\omega_0^4\left(\varphi_0^2 + 1\right)e^{-\omega_0\varphi_0 x}\left\{\left(\varphi_0^2 + 2\varphi_0 - 1\right)\cos(\omega_0 x) - \varphi_0\left(\varphi_0^2 - 2\varphi_0 - 1\right)\sin(\omega_0 x)\right\}, \quad x > 0 \tag{67}$$

Thus the right-hand side of the key differential equation (62) is

$$2N\frac{d^2v_0}{dx^2} = \Delta_b e^{-Dx}\left\{\Theta_1\cos(\omega_0 x) + \Theta_2\sin(\omega_0 x)\right\} \tag{68}$$

where

$$\Delta_b = 2N\delta_{b,0}\omega_0^2\left(\varphi_0^2 + 1\right), \quad D = \omega_0\varphi_0, \quad \Theta_1 = 1 \quad \text{and} \quad \Theta_2 = -\varphi_0 \tag{69}$$

Thus for $x > 0$, our key equation to solve is

$$\frac{d^4\tilde{v}}{dx^4} - 2N\frac{d^2\tilde{v}}{dx^2} + \Phi\tilde{v} = \Delta_b e^{-Dx}\left\{\Theta_1\cos(\omega_0 x) + \Theta_2\sin(\omega_0 x)\right\} \tag{70}$$

The four complementary solutions from solving the homogeneous equation (left-hand side set equal to zero) are the same in structure as obtained in solving (5), and given by

$$\tilde{v}_1 = e^{-\omega\varphi x}\cos(\omega x), \quad \tilde{v}_2 = e^{-\omega\varphi x}\sin(\omega x), \quad \tilde{v}_3 = e^{\omega\varphi x}\cos(\omega x) \text{ and } \tilde{v}_4 = e^{\omega\varphi x}\sin(\omega x) \tag{71}$$

We also require a particular solution, $\tilde{v}(x) = \tilde{v}_p(x)$, to (70) and by the method of undetermined coefficients we can work with the form

$$\tilde{v}_p = e^{-Dx}\left(P\cos(\omega_0 x) + Q\sin(\omega_0 x)\right) \tag{72}$$

where P and Q are constants to be solved for. Substitution of () into () leads (after considerable algebra) to

$$P = \frac{\Omega_1 \Theta_1 + \Omega_2 \Theta_2}{\Omega_1^2 + \Omega_2^2}\Delta_b \quad \text{and} \quad Q = \frac{\Omega_1 \Theta_2 - \Omega_2 \Theta_1}{\Omega_1^2 + \Omega_2^2}\Delta_b \tag{73}$$

where

$$\Omega_1 = D^4 - 6D^2\omega_0^2 + \omega_0^4 - 2ND^2 + 2N\omega_0^2 + \Phi \tag{74}$$

and

$$\Omega_2 = 4D^3\omega_0 - 4D\omega_0^3 - 4ND\omega_0 \tag{75}$$

The general solution for $x > 0$ is a linear combination of the complementary and particular solutions in the form

$$\tilde{v}(x) = C_1 e^{-\omega\varphi x}\cos(\omega x) + C_2 e^{-\omega\varphi x}\sin(\omega x) + C_3 e^{\omega\varphi x}\cos(\omega x) + C_4 e^{\omega\varphi x}\sin(\omega x)$$
$$+ e^{-\omega_0\varphi_0 x}\left(P\cos(\omega_0 x) + Q\sin(\omega_0 x)\right) \tag{76}$$

However, the solution must be bounded as $x \to \infty$ so we must have $C_3 = C_4 = 0$, leaving

$$\tilde{v}(x) = e^{-\omega\varphi x}\left(C_1\cos(\omega x) + C_2\sin(\omega x)\right) + e^{-\omega_0\varphi_0 x}\left(P\cos(\omega_0 x) + Q\sin(\omega_0 x)\right) \tag{77}$$

We can solve for the two unknown constants, C_1 and C_2 using the boundary conditions at $x = 0$ provided with (62). For this purpose we need several derivatives. These are

$$\frac{d\tilde{v}}{dx} = -e^{-\omega\varphi x}\left(C_1'\cos(\omega x) + C_2'\sin(\omega x)\right) - e^{-\omega_0\varphi_0 x}\left(P'\cos(\omega_0 x) + Q'\sin(\omega_0 x)\right) \tag{78}$$

where

$$C_1' = \omega(\varphi C_1 - C_2), \quad C_2' = \omega(\varphi C_2 + C_1), \tag{79}$$

$$P' = \omega_0(\varphi_0 P - Q), \quad Q' = \omega_0(\varphi_0 Q + P) \tag{80}$$

as well as

$$\frac{d^2\tilde{v}}{dx^2} = +e^{-\omega\varphi x}\left(C_1''\cos(\omega x) + C_2''\sin(\omega x)\right) + e^{-\omega_0\varphi_0 x}\left(P''\cos(\omega_0 x) + Q''\sin(\omega_0 x)\right) \tag{81}$$

where

$$C_1'' = (\omega^2\varphi^2 - \omega)C_1 - (\omega^2\varphi + \omega\varphi)C_2, \quad C_2'' = (\omega^2\varphi + \omega\varphi)C_1 + (\omega^2\varphi^2 - \omega)C_2 \tag{82}$$

$$P'' = (\omega_0^2\varphi_0^2 - \omega_0)P - (\omega_0^2\varphi_0 + \omega_0\varphi_0)Q, \quad Q'' = (\omega_0^2\varphi_0 + \omega_0\varphi_0)P + (\omega_0^2\varphi_0^2 - \omega_0)Q \tag{83}$$

and finally

$$\frac{d^3\tilde{v}}{dx^3} = -e^{-\omega\varphi x}\left(C_1'''\cos(\omega x) + C_2'''\sin(\omega x)\right) - e^{-\omega_0\varphi_0 x}\left(P'''\cos(\omega_0 x) + Q'''\sin(\omega_0 x)\right) \tag{84}$$

where

$$C_1''' = \left[(\omega^2\varphi^2 - \omega)\omega\varphi - (\omega^2\varphi + \omega\varphi)\omega\right]C_1 - \left[(\omega^2\varphi^2 - \omega)\omega + (\omega^2\varphi + \omega\varphi)\omega\varphi\right]C_2 \tag{85}$$

$$C_2''' = \left[(\omega^2\varphi + \omega\varphi)\omega\varphi + (\omega^2\varphi^2 - \omega)\omega\right]C_1 - \left[(\omega^2\varphi + \omega\varphi)\omega - (\omega^2\varphi^2 - \omega)\omega\varphi\right]C_2 \tag{86}$$

$$P''' = \left[(\omega_0^2\varphi_0^2 - \omega_0)\omega_0\varphi_0 - (\omega_0^2\varphi_0 + \omega_0\varphi_0)\omega_0\right]P - \left[(\omega_0^2\varphi_0^2 - \omega_0)\omega_0 + (\omega_0^2\varphi_0 + \omega_0\varphi_0)\omega_0\varphi_0\right]Q \tag{87}$$

$$Q''' = \left[(\omega_0^2\varphi_0 + \omega_0\varphi_0)\omega_0\varphi_0 + (\omega_0^2\varphi_0^2 - \omega_0)\omega_0\right]P - \left[(\omega_0^2\varphi_0 + \omega_0\varphi_0)\omega_0 - (\omega_0^2\varphi_0^2 - \omega_0)\omega_0\varphi_0\right]Q \tag{88}$$

Applying the boundary conditions, we first have zero slope condition at $x = 0$, that is

17

$$d\tilde{v}(0)\big/dx = -C_1' - P' = 0 \tag{89}$$

and the third derivative must be zero meaning there is no jump in the shear load so that

$$d^3\tilde{v}(0)\big/dx^3 = -C_1''' - P''' = 0 \tag{90}$$

These two equations result in $C_1' = -P'$, $C_1''' = -P'''$ and thus we obtain the simplification into two equations

$$\varphi\omega C_1 - \omega C_2 = -\omega_0\left(\varphi_0 P - Q\right) \tag{91}$$

and

$$\begin{aligned}
&\left[\left(\omega^2\varphi^2 - \omega\right)\omega\varphi - \left(\omega^2\varphi + \omega\varphi\right)\omega\right]C_1 - \left[\left(\omega^2\varphi^2 - \omega\right)\omega + \left(\omega^2\varphi + \omega\varphi\right)\omega\varphi\right]C_2 \\
&= -\left[\left(\omega_0^2\varphi_0^2 - \omega_0\right)\omega_0\varphi_0 - \left(\omega_0^2\varphi_0 + \omega_0\varphi_0\right)\omega_0\right]P - \left[\left(\omega_0^2\varphi_0^2 - \omega_0\right)\omega_0 + \left(\omega_0^2\varphi_0 + \omega_0\varphi_0\right)\omega_0\varphi_0\right]Q
\end{aligned} \tag{92}$$

in two unknowns, C_1 and C_2. Letting

$$A_{11} = \varphi\omega \quad \text{and} \quad A_{12} = -\omega \tag{93}$$

$$A_{21} = \left[\left(\omega^2\varphi^2 - \omega\right)\omega\varphi - \left(\omega^2\varphi + \omega\varphi\right)\omega\right] \quad \text{and} \quad A_{22} = -\left[\left(\omega^2\varphi^2 - \omega\right)\omega + \left(\omega^2\varphi + \omega\varphi\right)\omega\varphi\right] \tag{94}$$

$$B_1 = -\left(\omega_0\varphi_0 P - \omega_0 Q\right) \tag{95}$$

and

$$B_2 = -\left[\left(\omega_0^2\varphi_0^2 - \omega_0\right)\omega_0\varphi_0 - \left(\omega_0^2\varphi_0 + \omega_0\varphi_0\right)\omega_0\right]P + \left[\left(\omega_0^2\varphi_0^2 - \omega_0\right)\omega_0 + \left(\omega_0^2\varphi_0 + \omega_0\varphi_0\right)\omega_0\varphi_0\right]Q \tag{96}$$

and using Cramer's rule on (91) and (92), the solutions for C_1 and C_2 are

$$C_1 = \frac{A_{22}B_1 - A_{12}B_2}{A_{11}A_{22} - A_{21}A_{12}} \quad \text{and} \quad C_2 = \frac{-A_{21}B_1 + A_{11}B_2}{A_{11}A_{22} - A_{21}A_{12}} \tag{97}$$

Thus our solution for $x > 0$ is

$$\tilde{v}(x) = e^{-\omega\varphi x}\left(C_1\cos(\omega x) + C_2\sin(\omega x)\right) + e^{-\omega_0\varphi_0 x}\left(P\cos(\omega_0 x) + Q\sin(\omega_0 x)\right), \; x > 0 \tag{98}$$

We also require the bending moments and these depend on the curvature given by

$$\frac{d^2\tilde{v}}{dx^2} = +e^{-\omega\varphi x}\left(C_1''\cos(\omega x) + C_2''\sin(\omega x)\right) + e^{-\omega_0\varphi_0 x}\left(P''\cos(\omega_0 x) + Q''\sin(\omega_0 x)\right), \; x > 0 \tag{99}$$

where

$$C_1'' = \left(\omega^2\varphi^2 - \omega\right)C_1 - \left(\omega^2\varphi + \omega\varphi\right)C_2, \quad C_2'' = \left(\omega^2\varphi + \omega\varphi\right)C_1 + \left(\omega^2\varphi^2 - \omega\right)C_2 \tag{100}$$

$$P'' = \left(\omega_0^2\varphi_0^2 - \omega_0\right)P - \left(\omega_0^2\varphi_0 + \omega_0\varphi_0\right)Q \quad \text{and} \quad Q'' = \left(\omega_0^2\varphi_0 + \omega_0\varphi_0\right)P + \left(\omega_0^2\varphi_0^2 - \omega_0\right)Q \tag{101}$$

We can extend the solution to $-\infty < x < \infty$ by writing

$$\tilde{v}(x) = e^{-\omega\varphi|x|}\left(C_1\cos(\omega x) + C_2\sin(\omega|x|)\right) + e^{-\omega_0\varphi_0|x|}\left(P\cos(\omega_0 x) + Q\sin(\omega_0|x|)\right), \; -\infty < x < \infty \tag{102}$$

and

$$\frac{d^2\tilde{v}}{dx^2} = +e^{-\omega\varphi x}\left(C_1''\cos(\omega x) + C_2''\sin(\omega|x|)\right) + e^{-\omega_0\varphi_0 x}\left(P''\cos(\omega_0 x) + Q''\sin(\omega_0|x|)\right), \; -\infty < x < \infty \tag{103}$$

The last two equations represent the key results of the derivation, and allow us to calculate the changes in transverse liner displacement, interface pressure and bending moments caused by the frozen in transverse displacement of the liner inherited from autofrettage.

F. Procedure for Calculating Displacements, Moments and Contact Pressures at Zero Vessel Pressure.

Because of the structure of the fundamental differential equation (62), it is necessary to specify a reference state where the liner tension is zero, $N_l = N = 0$ and the frozen-in displacement profile is $v_0(x)$. Otherwise, at any other value of N_l and corresponding value of N, the displacement profile will be $v(x) = \tilde{v}(x) + v_0(x)$ and will not

match the reference state on the right hand side of (62). This would considerably complicate the analysis, since the development of the displacement disturbance (depression) from void compaction occurs primarily at some effective liner tension, denoted $N_{l,c}$, close to the liner tension at peak proof pressure, denoted $N_{l,p}$. (This is chosen slightly different from $N_{l,p}$ to allow some flexibility in adjusting the reference depression shape, $v_0(x)$.) Furthermore, the liner yielding causing relaxation of the bending moment and dispersion in the contact pressure around the initial very narrow and very stiff region, also occurs at the liner tension, $N_{l,p}$, at peak proof pressure. Thus we must consider the unloading phase from $N_l = N_{l,p}$ to $N_l = 0$ in order to determine the conditions that exist at peak proof pressure compared to the reference state. Once appropriately determined, we can reduce the liner tension from $N_l = 0$ to $N_l = N_{l,u}$, which is a negative value corresponding to 0 psi vessel pressure, and estimate the displacement, moment and contact pressure conditions that apply there.

An important point to note is that the measurement of the depression depth profile and maximum value, $\delta_{b,u}$, is typically performed at zero vessel pressure using a profilometer or eddy current probe. Thus whatever parameters are chosen to determine the reference state and state at proof, they must result in this measured profile. What is found is that the liner depression displacements are largest at zero vessel pressure ($N_l = N_{l,u}$, $\delta_b = \delta_{b,u}$), only 2 to 5% smaller at the zero-tension liner state ($N_l = 0$, $\delta_b = \delta_{b,0}$), corresponding to about 2650 psi in a 40 inch vessel, and are an additional 12 to 20% smaller at the full proof pressure ($N_l = N_{l,p}$, $\delta_b = \delta_{b,p}$). While small, these differences are important to consider during modeling for possible buckling.

Earlier we derived a result for the frozen-in displacement profile at $N_l = 0$, given by (57). This shape corresponded to a sharp line displacement or equivalent force per unit length (transverse to the line of the in-plane load) of maximum reference depth magnitude, $\delta_{b,0}$, assuming model parameters based on the initially low transverse stiffness of the overwrap, $E_{O,t,0}$, since this is what prevailed when the depression was formed at $N_l = N_{l,c}$. One might question whether the line force ought to be replaced by the dispersed pressure version, but this would greatly complicate an already complicated analysis with little benefit since it makes virtually no difference to the reference, frozen-in displacement profile, $v_0(x)$, at $N_l = 0$. Also, once the frozen-in deformation occurs at $N_l = N_{l,c}$, we assume the overwrap stiffness is the same everywhere and now has the stiffened state $E_{O,t} \gg E_{O,t,0}$. Thus, changes to the bending moment profile, when N_l is increased or decreased relative to $N_l = 0$, are smooth and involve no discontinuity in slope (as occurs for instance in three-point bending). This calculation was the heart of the latest calculation.

Finally, we must treat the residual bending moment and associated interface pressure disturbance that results when the compaction occurs at an effective liner tension $N_l = N_{l,c} \approx N_{l,p}$ at maximum displacement $\delta_{b,p}$ corresponding to maximum proof pressure. This calculation, performed earlier began with parameters associated with the transversely soft overwrap state, $E_{O,t,0}$, and a sharp line load corresponding to displacement, $\delta_{b,p}$. Calculating the nominal pressure profile assuming bending in the elastic state, requires obtaining the fourth derivative of displacement. In keeping with equilibrium, it was found that the pressure profile involved a force component applied as a Dirac delta function along the applied line displacement of magnitude, $\delta_{b,p}$. Using a fourth order polynomial (46), dominated by a second order parabola, the line-force was redistributed as a parabolic like pressure distribution, with the fourth order terms providing continuity in displacement and slope at the boundaries of this pressure distribution. Additionally, the nominally elastic bending moment distribution were relaxed to about half because of the plastic yielding occurring during autofrettage, which completely blunted half of the stress perturbation from bending. Also for higher depression displacements, a plastic limit in bending was assumed to occur, restricting the maximum bending moment that can exist at proof. Once the form of the pressure distribution was known, the bending moment distribution could be calculated, and a relationship between the maximum pressure, width of the dispersed force and maximum bending moment could be calculated.

Thus the calculation proceeds by first estimating the maximum displacement difference that would occur between the reference state $N_l = 0$ and proof state $N_l = N_{l,p}$, using the solutions developed from (57) to (103). In other words, $\delta_{b,p} = \delta_{b,0} - \tilde{v}(0, N_{l,p})$. Once $\delta_{b,p}$ is known, we calculate the residual bending moment distribution,

$M_p(x)$, and interface pressure distribution, $p_p(x)$, with reference to this state of maximum liner tension at proof. Then using the moment and displacement solution with reference to $N_l = 0$, we can calculate the change in bending moment distribution and pressure distribution in unloading from $N_l = N_{l,p}$ to $N_l = 0$. Then, as a final step, we can reduce the liner tension from $N_l = 0$ to $N_l = N_{l,u}$ corresponding to zero vessel pressure. The results for the final moment distribution, pressure distribution and displacement profiles are

$$M_u(x) = M_c(x) + K_p EI \left(\frac{d^2}{dx^2} \tilde{v}(x; N_{l,u}) - \frac{d^2}{dx^2} \tilde{v}(x; N_{l,p}) \right) \tag{104}$$

$$p_u(x) = p_p(x) + \frac{E_{O,t}(1 - v_l^2)}{t_O} \{ \tilde{v}(x; N_{l,u}) - \tilde{v}(x; N_{l,p}) \} \tag{105}$$

and finally

$$v(x) = v_0(x) + \tilde{v}(x; N_l) \tag{106}$$

The critical conditions for the onset of buckling involve searching for cases with two critical properties: First is that the liner pressure goes negative, i.e., the interface has tensile tractions, which cannot be sustained since the overwrap is not glued to the liner and the second is that the bending moments have zero points more than two inches apart spanning the negative pressure region. When both these conditions exist, it is possible for buckling to occur.

V.   Results of Model Calculations on Potential for OMS Liner Buckling

We now present graphical results from the above analysis for a 40 inch Kevlar/epoxy spherical COPV, with titanium liner of thickness, $t_l = 0.106$ in., Young's modulus, $E_l = 16.5 \times 10^6$ psi, and Poisson's ratio, $v_l = 0.342$. The maximum possible value for N_l during autofrettage is determined from the liner yield stress, $\sigma_{l,y} = 128,000$ psi as $N_{l,p} = \sigma_{l,y} t_l = 13,570$ lb/in. The liner compressive load at zero pressure after autofrettage is nominally $N_{l,u} = -9,172$ lb/in. In the mathematical calculations, a reference state of zero liner tension, $N_l = 0$ lb/in., was chosen, which happens to corresponds to 2,650 psi pressure in the vessel after autofrettage. Choice of this reference state greatly simplified the mathematical analysis, but has no effect on the predicted results and conclusions.

Based on the analytical results for depression displacement, $v(x)$, at liner tension, N_l, after autofrettage, Figure 5 is the predicted profile from a 40 mil depression in 40 in. liner corresponding to the reference state at zero liner tension, $N_l = 0$ lb/in., at a vessel pressure of 2,650 psi following autofrettage. The depression depth is measured relative to an equilibrium radial deformation state for a perfect sphere, balancing the vessel pressure and the liner and overwrap tension. In the formation of this depression during initial pressurization, the through-thickness stiffness of the overwrap was taken as $E_{O,t,0} = 25,000$ psi, representing the pre-proof state with voids (and consistent with the result from the special OMS vessel tested in 1977 at JSC).

For the unloading phase from the peak proof pressure of 6,520 psi, and peak liner tension $N_{l,p} = 13,570$ lb/in. the through thickness stiffness of the overwrap was increased to $E_{O,t} = 250,000$ psi, due to overwrap compaction consistent with experiments at WSTF using eddy current probes. The resulting depression width (half-wavelength) of about 5 inches matches well the experimental width measured by laser profilometry in Figure 3. Note that under the full tension of the proof pressure, the depression depth of about 37.75 mils is less than the 40 mil reference depth at zero tension, and under full liner compression at 0 psi vessel pressure, the peak displacement is 42.25 mils, slightly larger than the 40 mil reference depth. These differences are relatively small because of the greatly increased through-thickness overwrap stiffness once void compaction is complete.

Note also that the incremental profiles representing *changes* in displacement measured relative to the reference state have much shorter half- wavelengths than the originally formed depression, again because of this greatly increased overwrap stiffness. This mismatch in half-wavelength turns out to be a very important feature in controlling the onset of buckling.
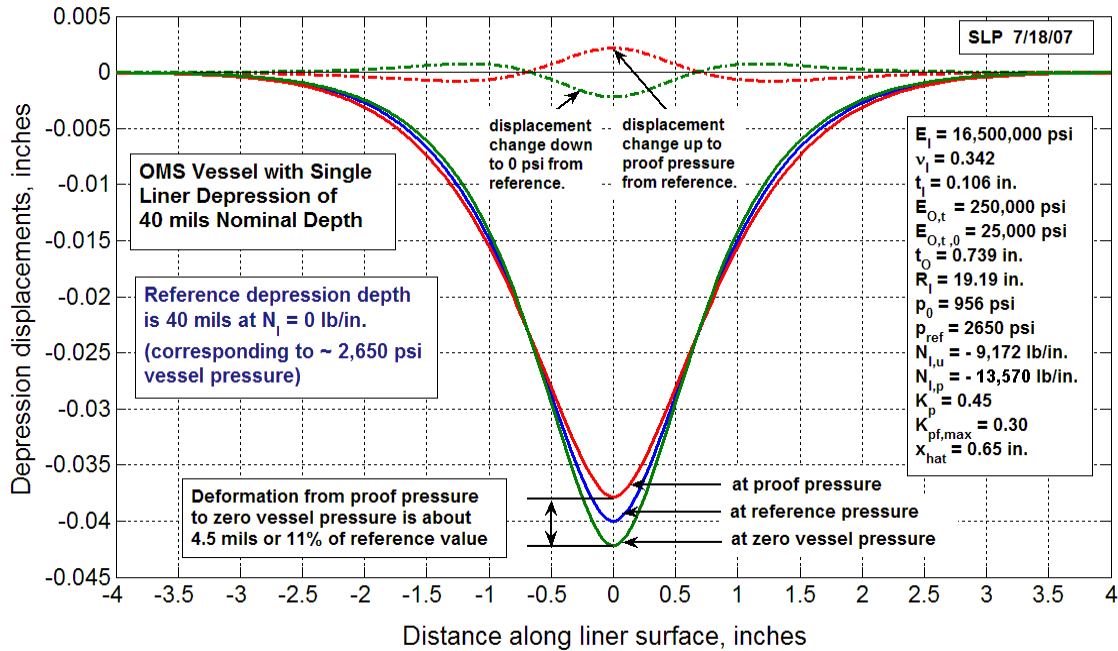
Figure 5. Predicted characteristics of the displacement profile in an OMS liner due to a nominal 40 mil depression and shown at the reference state and the states of proof pressure and zero pressure after proof.
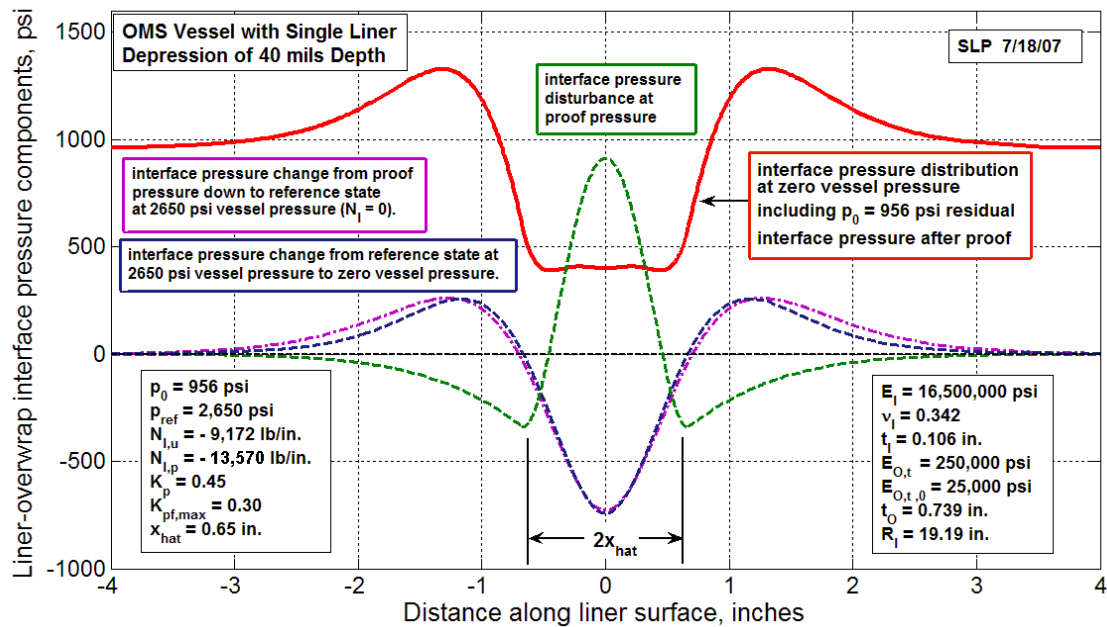

Figure 6. Predicted characteristics of the interface pressure profile in an OMS liner due to a nominal 40 mil depression and calculated at the proof pressure and at zero pressure after proof.

Figure 6 shows the predicted interface pressure profile in an OMS vessel from a 40 mil (0.040 in.) depression corresponding to the displacement profiles in Figure 5. This includes the nominal or average interface pressure bias, $p_0 = 956$ psi at zero vessel pressure, which results from radial interference of the overwrap and liner induced by plastic yielding of the latter during autofrettage. Also shown is the state of the interface pressure profile at the peak proof pressure of 6520 psi, and $N_{l,p} = 13,570$ lb/in. as well as the changes in interface pressure from the proof pressure to the reference state of zero liner tension (at 2650 psi), and from this reference state down to zero vessel

American Institute of Aeronautics and Astronautics

pressure. Note that the delta function spike in pressure due to the idealized line load at proof pressure evolves into a more dispersed, approximately parabolic profile from $|\hat{x}| \leq 0.65$ in. A key observation is that the interface pressure drops to about 400 psi over close to a 1.3 inch region centered over the depression. Still there remains a reserve of interface pressure to maintain firm contact between the overwrap liner thus maintaining elastic stability.

Figure 7 shows the calculated bending moments associated with the 40 mil depression under the conditions of Figures 5 and 6. Shown are the bending moment distribution at the peak autofrettage pressure as well as the changes in bending moment upon reducing pressure to the reference state of zero tension in the liner at 2650 psi, and then from this reference state down to the fully unloaded state of zero vessel pressure.   We sum the two latter components to obtain the total change in bending moment distribution from proof to zero vessel pressure, as well as the final bending moment distribution upon summing all components.

An important observation in Figure 7 is that magnitude of the change in maximum bending moment coming down from the peak proof pressure differs very little from the final magnitude. Thus, unlike the situation with the interface pressure, the magnitude of the residual bending moment at proof has little influence on the final bending moment at zero vessel pressure. The zero moment hinge points are considerably wider than 2.0 inches meaning that significant benefit of overwrap support exists outside of rage the reduced interface pressure. However the final bending moment is large enough to impinge on the limitations imposed by the Bauschinger effect, and even if the final bending moment might increase with an increase in depression depth, say to 50 mils, softening in the liner is likely in bending as reflected by a reduced secant modulus seen in Figure 4.
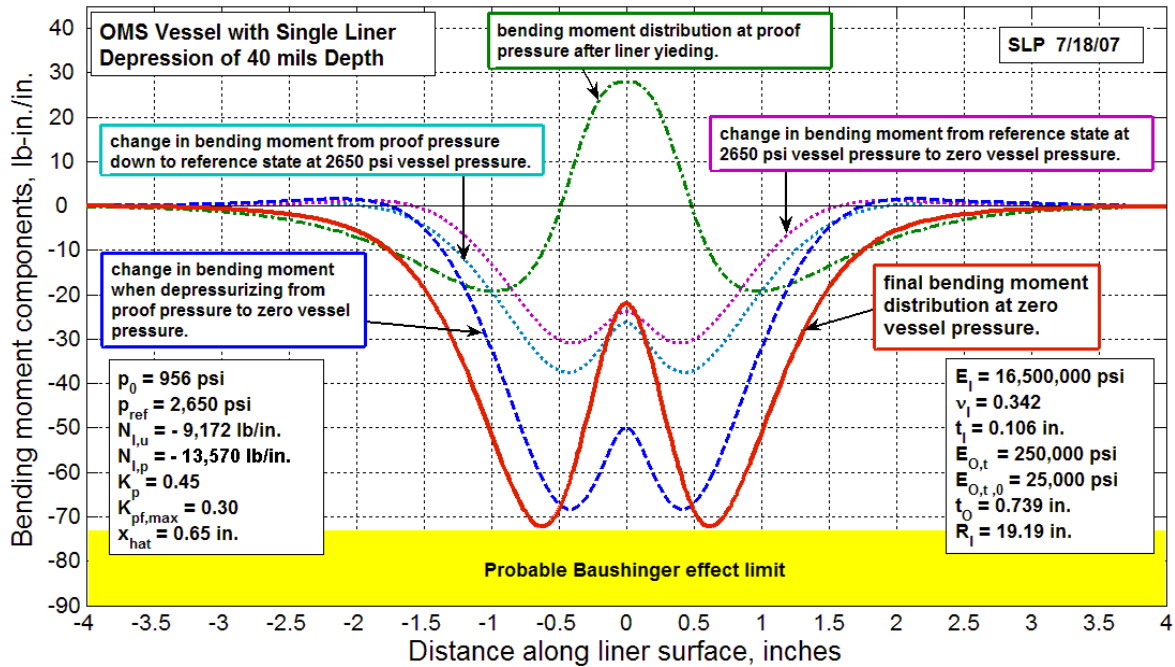

Figure 7. Predicted characteristics of the bending moment profiles in an OMS liner due to a nominal 40 mil depression and calculated at the proof pressure and at zero pressure after proof.

Figure 8 shows the change in interface pressure that results at 40 mils depression depth when the effective liner stiffness (secant) is reduced 15% from 16.5 Msi to 14.0 Msi. This change is enough to reduce the interface pressure to zero over a substantial region spanning the depression, thus resulting in critical conditions for liner separation. The same loss in secant stiffness of the liner material in bending leads to further increases in elastically calculated bending moment, as shown in Figure 9. This signals an unstable state where yielding due to the Bauschinger effect on depressurization does not lead to bending moment relief but rather runaway deformation signaling liner collapse.
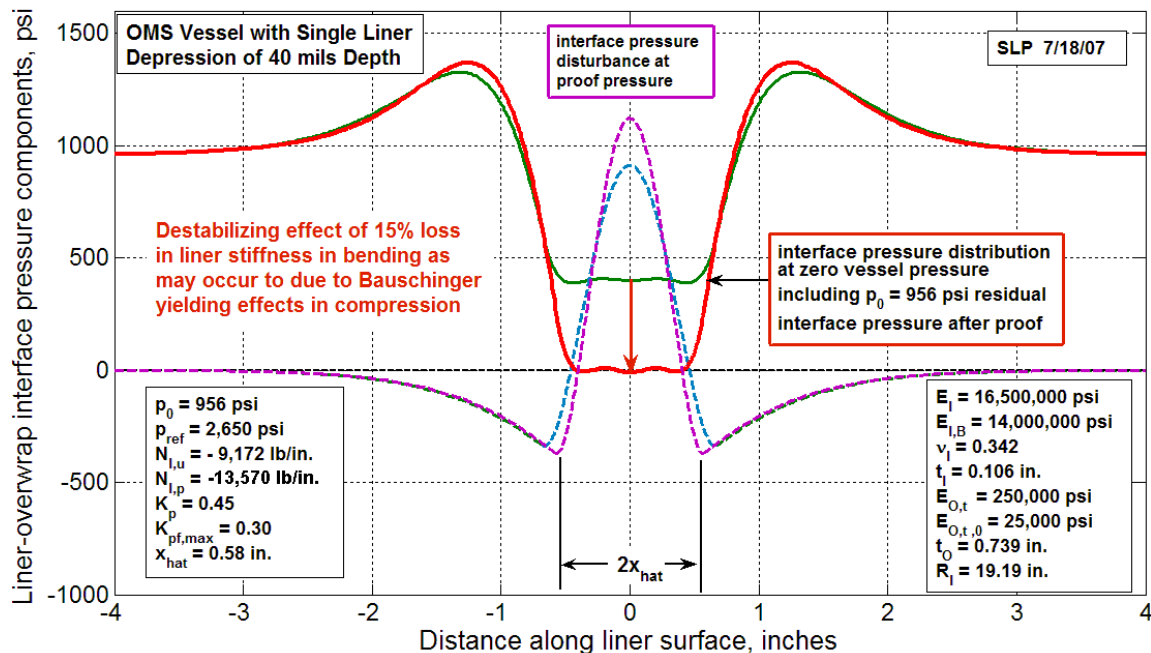
Figure 8. Effect on interface pressure of reducing the liner stiffness 15% from 16.5 Msi to 14.0 Msi, when the nominal depression depth is 40 mils.
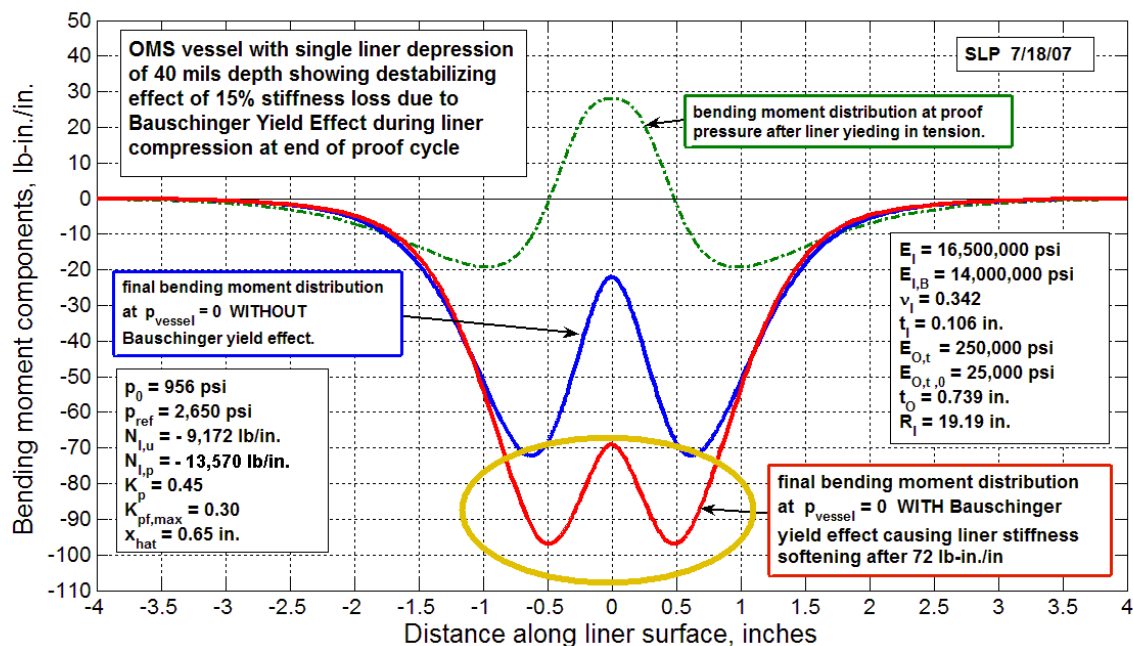

Figure 9. Effect on the bending moment of reducing the liner stiffness 15% from 16.5 Msi to 14.0 Msi, when the nominal depression depth is 40 mils.

The Bauschinger limit imposed in Figure 7 may be conservative, so we consider the sensitivity of these results to changes in the depression depth. Figures 10 and 11 show the effects of changing the depression depth for the cases in Figures 5 through 7 and returning to a liner stiffness of 16.5 Msi. Clearly it is highly unlikely for the liner to be stable at depression depths above about 55 mils irrespective of the details of Bauschinger yielding effects.
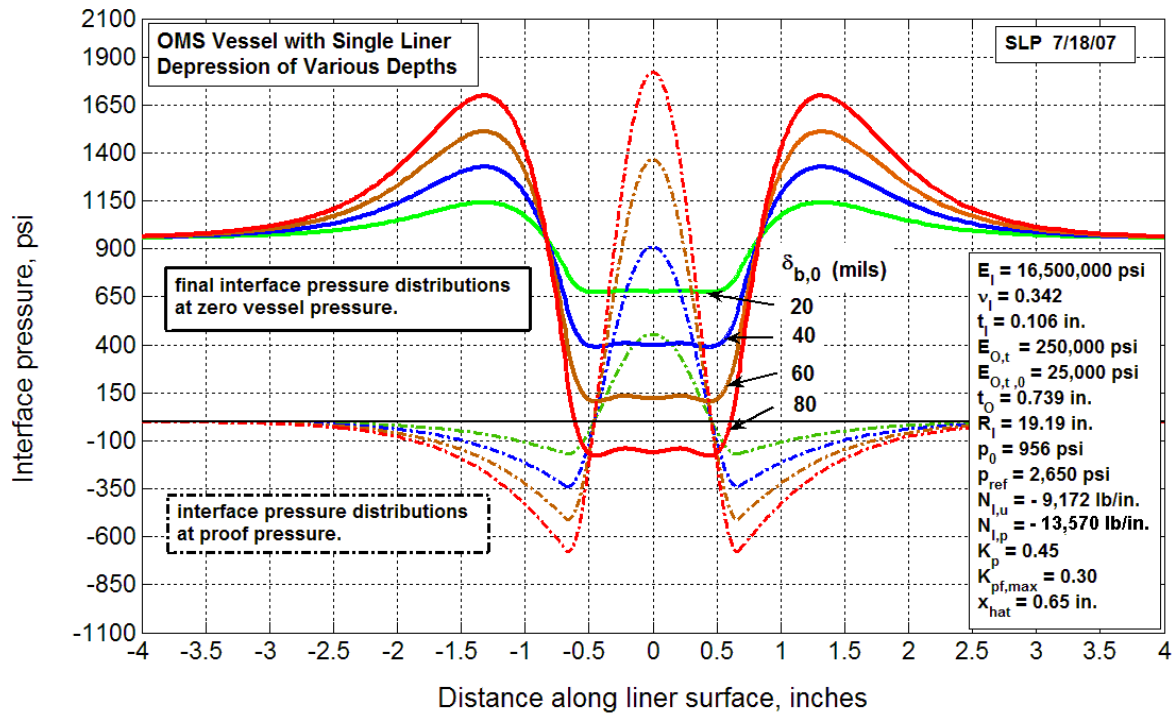
Figure 10. Effect on the nominal interface pressure distribution in an unpressurized vessel of changing the nominal depression depth over a range from 20 mils to 80 mils.
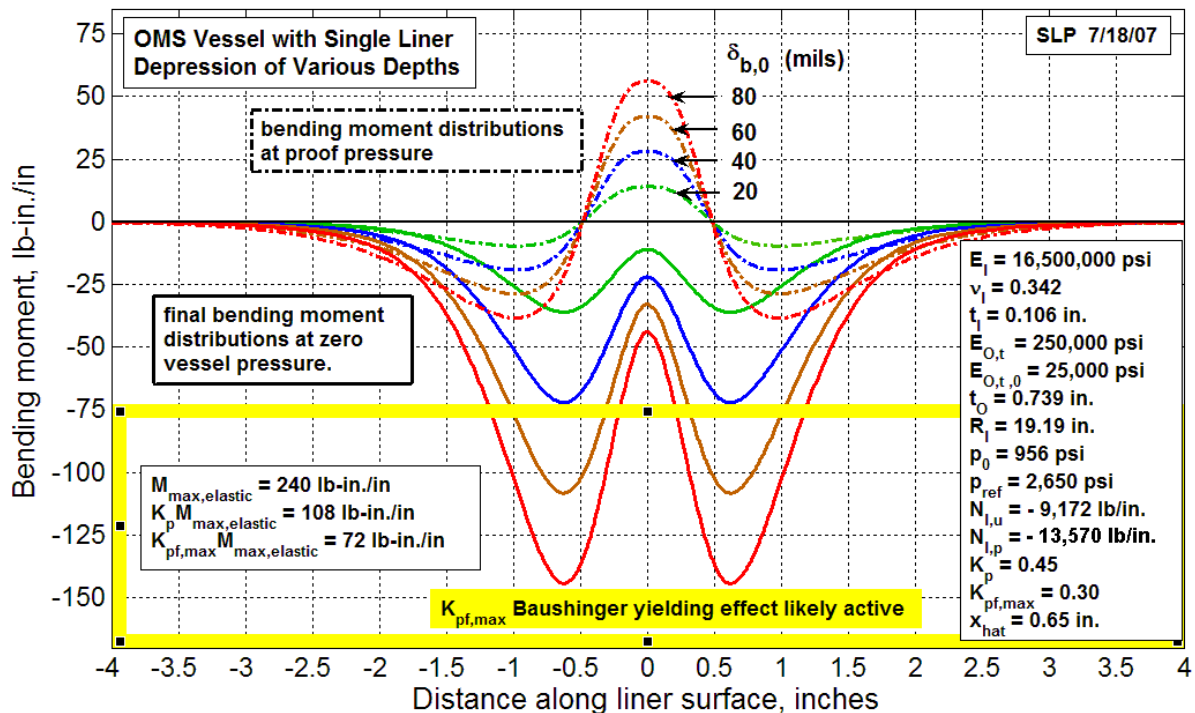

Figure 11. Effect on the nominal (elastic) bending moment distribution in an unpressurized vessel of changing the nominal depression depth from 20 mils to 80 mils.

American Institute of Aeronautics and Astronautics

VI. Concluding Comments

A key observation is that the magnitude of the change in maximum bending moment when depressurizing from the peak proof pressure differs little from the final magnitude. Thus, unlike the situation with the interface pressure, the magnitude of the residual bending moment at proof has little influence on the final bending moment at zero vessel pressure. The zero moment hinge points are considerably wider than 2.0 inches meaning that significant benefit of overwrap support exists outside of range of the reduced interface pressure. However, the final bending moment is large enough to impinge on the limitations imposed by the Bauschinger effect, and even if the final bending moment were to increase with increased depression depth, softening in the liner is likely in bending as reflected by a reduced secant modulus.

The main conclusion is that the liner is likely to stable and not buckle from depression depths of up to about 40 mils. Fortunately this depth is double the depression depths of about 20 mils that have been observed using laser profilometry, and are believed a characteristic of the winding process.   Figures 10 and 11 indicate that a nominal depression depth of 20 mils (actual about 21 mils) presents no hazard. Above 40 mils, the Bauschinger effect becomes extremely important and destabilization and buckling becomes increasingly likely depending on the details of depression formation during the proof pressurization. Whatever the mechanical property variations for a particular vessel, it appears almost certain that destabilization and buckling will occur for depression depths after proof beyond 55 mils, and beyond 40 mils there is considerable risk.

Acknowledgments

References

[1] Saulsberry, R.L.*, Private communication of results from experiments at NASA JSC White Sands Test Facility*, 2007.
[2] Thesken, J.C.*, Private communication of results from experiments at NASA Glenn Research Center*, 2007.